Hydrogeology Journal
https://doi.org/10.1007/s10040-024-02782-2

REPORT

Present and paleo-hydrogeological reconstruction of a complex deep groundwater system in a tectonically active region (Golan Heights, Middle East)

Hadas Ben-nun Levanon[1,2] · Avihu Burg[2] · Ittai Gavrieli[2] · Yoav O. Rosenberg[2] · Ronen Gersman[3] · Yuval Bartov[4] · Yakov Livshitz[5] · Avraham Starinsky[1] · Itay J. Reznik[2]

Received: 6 July 2023 / Accepted: 27 February 2024

Abstract

The geochemical and isotopic composition of deep groundwater in sedimentary aquitards reveals a complex paleo-hydrological system affected by intensive tectonic activity. Water samples collected from deep research boreholes in the Golan Heights (Middle East) exhibit a unique combination of high salinity (>2,000 mg/L Cl) with low Na/Cl (<0.7) and Mg/Ca (<0.3) equivalent ratios, calcium chloride water type [$Ca > (HCO_3 + SO_4)$], relatively low $\delta^{18}O_{VSMOW}$ and $\delta^{2}H_{VSMOW}$ values (–7 and –42‰, respectively), and enriched $^{87}Sr/^{86}Sr$ ratios compared to the host rocks. The salinity source is related to ancient lagoonary hypersaline brines (10–5 Ma) that existed along the Dead Sea Rift (DSR). These brines intruded into the rocks surrounding the DSR and, based on the current study, also extended away from the rift. Following their subsurface intrusion, the brines have been gradually diluted by ^{18}O- and ^{2}H-depleted freshwater recharged at high elevations, nowadays leaving only traces of the brines that originally intruded. It is also shown that variable hydraulic conductivities in different formations control the dilution rates and subsequently the preservation of the entrapped brines. A paleo-hydrological reconstruction is provided to demonstrate intrusion and backflow dynamics and also the relationship to freshwater dilution, which was triggered by a tectonically active basin of the nearby continental DSR. Brines that initially migrated from the rift have since been gradually flushed back to the rift through the current natural outlets. As the system discharges, it mixes and converges with a separate hydrogeological system, while still preserving some of the geochemical signals of the ancient brines.

Keywords Paleohydrology · Saltwater-freshwater interactions · Deep groundwater · Ca-chloride brines · Golan Heights

Introduction

Sedimentary basins often contain saline fluids in their deepest parts (Davisson and Criss 1996; Dickey 1969; Kreitler 1989). In some cases, saline fluids can persist in deep hydrogeological systems over millions of years, even in the presence of active regional groundwater flow (Bethke and Marshak 1990; Ferguson et al. 2018). Saline fluids exhibit different compositions depending on their origin and water–rock interaction processes. Some are remnants of water that was trapped in the pores during deposition (connate water), while others intruded later into the pore space. Saline intrusion can originate from various surface saltwater bodies (seawater, lagoons, salt lakes, etc.), or subsurface saline water bodies, which could be sourced from deeper strata and/or dissolution of highly soluble minerals (Bozau et al. 2015; Gaupp et al. 2008; Mirzavand et al. 2020). Thus, understanding the genesis of the saline fluids in the deeper parts of sedimentary basins can provide insights into the hydrological and chemical processes that have taken place in the subsurface, as well as the geological settings that enabled their intrusion and preservation in the system (Hanor 1994; Kharaka et al. 2007; Land 1995).

✉ Itay J. Reznik
reznik@gsi.gov.il

1 Institute of Earth Sciences, The Hebrew University of Jerusalem, 9190401 Jerusalem, Israel

2 Geological Survey of Israel, 32 Yesha'ayahu Leibowitz, 9692100 Jerusalem, Israel

3 Genie Oil and Gas Ltd., 5 Shlomo Halevi, 9777019 Jerusalem, Israel

4 MOSESTRO Exploration LLP, Shilat, Israel

5 Israeli Hydrological Service, Israeli Water Authority, 7 Bank Israel, Jerusalem 9195021, Israel

Published online: 17 April 2024

Deep formation waters in sedimentary basins are commonly saline and characterized by a Ca-chloride composition where Ca^{2+} concentrations are higher than the sum of (HCO_3^- and SO_4^{2-}) concentrations (meq/L), while Na/Cl ratios are lower than the marine value (0.86) (Carpenter 1978; Hanor 1994; Starinsky 1974). Therefore, the chemical composition of Ca-chloride water is distinguishably different from plain seawater, or evaporated seawater. Saline Ca-chloride waters are found around the world in sedimentary basins (Bozau et al. 2015; Maghrebi et al. 2021), rift zones (Hardie 1983; Klein-BenDavid et al. 2004; Starinsky and Katz 2014), oilfields (Carpenter 1978; Egeberg and Aagaard 1989; Hanor and McIntosh 2007; Land 1995; Stueber and Walter 1991) and hydrothermal systems (Aulstead and Spencer 1985).

Previous studies (Carpenter 1978; Starinsky 1974) proposed that saline Ca-chloride brines in sedimentary basins originate from seawater that underwent evaporation (i.e., evaporation by a factor of ≥10) and/or mineral precipitation (aragonite, gypsum, halite), followed by water–rock interactions such as epigenetic dolomitization and gypsum formation (Ilani et al. 1988; Shelton et al. 2009; Stein et al. 2002). The evaporation produces highly dense hypersaline brines that intrude by density-driven migration into the subsurface (Bąbel and Schreiber 2014; Katz and Starinsky 2009; Stanislavsky and Gvirtzman 1999). Once the brines have intruded the subsurface, they can remain stagnant in the deep parts of the sedimentary basins for very long periods, up to tens of millions of years (Hanor 1994; Lowenstein et al. 2003). Alternatively, if conditions allow, they can be diluted or flushed by a different water source (Aulstead and Spencer 1985; Ferguson et al. 2018; Kim et al. 2022; Spencer 1987). The timescale of flushing large sedimentary basins can be in the order of millions of years (Darrah et al. 2015; Deming and Nunn 1991).

Hydrogeological and geochemical data collected from 4 new research boreholes (Ness wells, Fig. 1) provided information regarding the composition and sources of previously unexplored deep-seated aquitard sedimentary units. The water in those units contained traces of Ca-chloride brines, which were diluted by freshwater. Based on the data, the goal of the study was to reconstruct the paleo-hydrogeological history and determine the present conditions of these deep groundwater systems as affected by a tectonically active continental rift (Dead Sea Transform).

Study area

Geological background

The Golan Heights (GH), located in the Middle East (Fig. 1a), is a sedimentary syncline that was covered during the Pliocene–Pleistocene by basaltic flows (Fig. 1b; Mor 1993; Sneh and Weinberger 2003). The sedimentary sequence underlying the basalts is exposed only at the northern and southern margins of the syncline, at the slopes of the Hermon and Ajloun anticlines, respectively (Fig. 1b). The western margin of the syncline is the active tectonic plate boundary of the Dead Sea Rift (DSR), which separates between the Arabian (east) plate and the African/Sinai (west) plate/subplate (Freund et al. 1968; Salamon et al. 2003; Shulman et al. 2004). The activity of the Dead Sea Rift transform resulted in a total left lateral displacement of 105 km between the plates (Quennell 1956). Activity over the past 25 Ma resulted in a 35–40-km shift (Freund et al. 1968; Walley 1998). The transform also branched eastwards towards the Golan area into several divergent faults, such as the Shamir and Sheikh Ali faults (Fig. 1b), which led to the discontinuation of the syncline structure and to the exhumation of the uplifted structure of the Hermon Anticline (Garfunkel 1981; Meiler et al. 2011; Ron et al. 1984).

The sedimentary section in the study area (Figs. 1, 2 and 3) consists of a thick Jurassic section (Arad Group), composed mostly of limestones, which constitutes most of the Hermon exposures. Units from the Cretaceous are composed of sandstones (Kurnub Group, Lower Cretaceous), dolomites and limestones (Judea Group, Upper Cretaceous; Michelson 1979; Sneh et al. 1998). Overlying the Judea Group is the Senonian Mt. Scopus Group. The base of the Mt. Scopus Group (Menuha Formation) is composed of massive white chalk (Mimran et al. 1985). The overlying Mishash Formation consists of chalk-chert alterations at its lower part (Margane et al. 2002; Mimran et al. 1985). The Upper Mishash and Ghareb formations are mostly inseparable and are composed of chalk. The Senonian rocks are considered to be extremely organic rich Type II-S source rocks that have partially matured from a paleo-thermal event (Reznik and Bartov 2021) and currently contain viscous immovable bituminous material (Rosenberg et al. 2017; Rosenberg and Reznik 2021). The uppermost Taqiye Formation of the Mt. Scopus Group is distinguishable from the underlying sequence, since it is consistently composed of marly chalk and lacks organic matter (Flexer and Honigstein 1984; Margane et al. 2002; Mimran et al. 1985).

Though the Mt. Scopus Group is barely exposed at the surface in the GH north of the Lower Yarmouk Gorge (LYG), it is widely exposed to the south of the Yarmouk, at the Ajloun anticline (Fig. 1b). Overlying the Mt. Scopus Group are the Eocene chalks (Avedat Group) and the Neogene conglomerates and clay (Hordos Formation), representing a shift from a marine to a terrestrial environment (Sneh 1996). The top of the sedimentary section of the GH is marked by thick basaltic flows from the Pliocene–Pleistocene (Bashan Group). Most of the surface of the southern GH is covered by the basaltic flows from the Pliocene (5–3

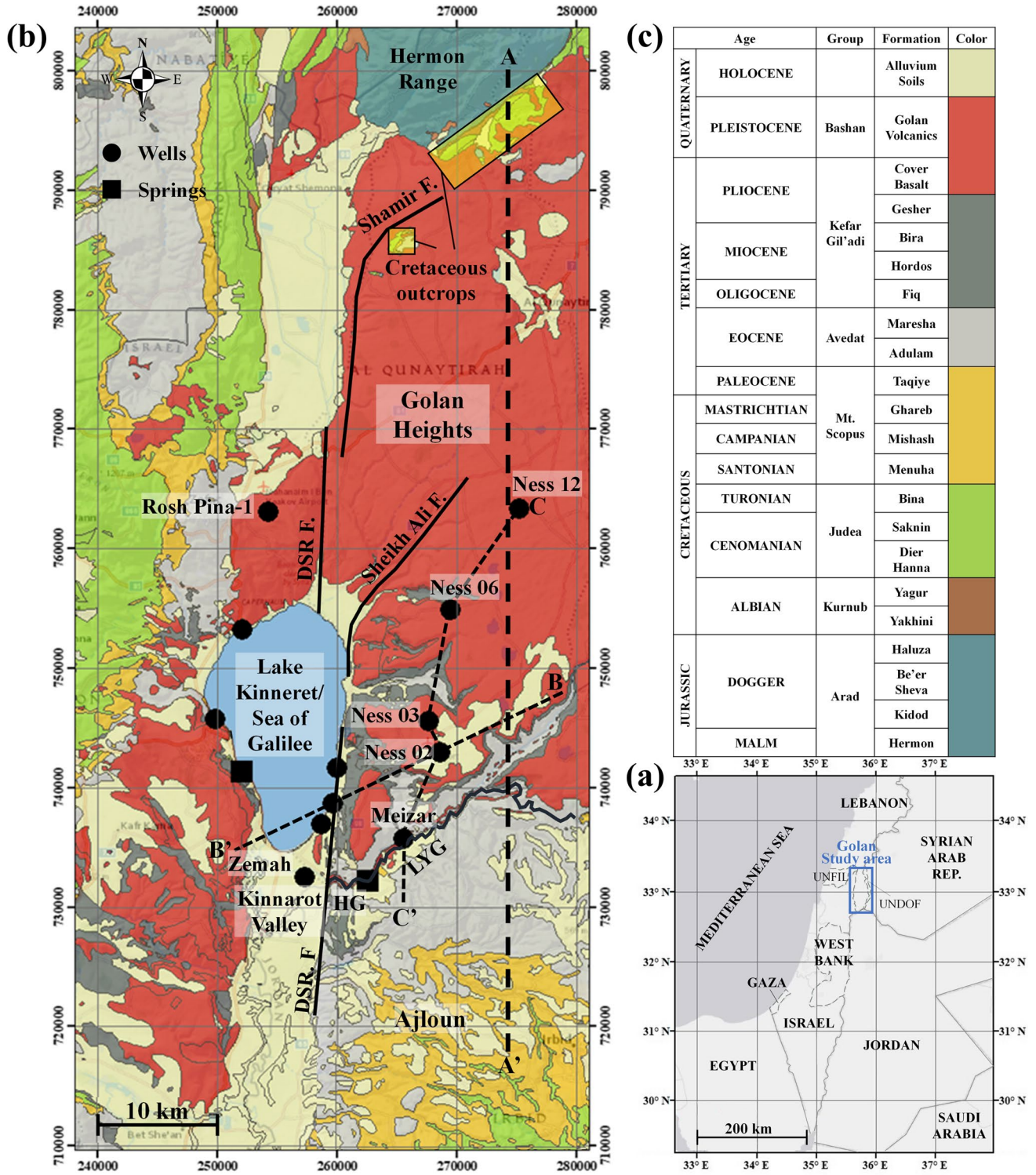

Fig. 1 **a** General location of the study area, modified after UN (2023), and **b** locations of water sources on top of a geological map (New Israel Grid Coordinates). Colors correspond to the stratigraphic table (**c**). The main outcrop of the Mt. Scopus and Judea groups at the foothills of Mt. Hermon are highlighted in yellow (Cretaceous outcrops). Dashed lines (A–A′ and B-B') mark the location of the cross sections in Figs. 2 and 3, respectively. DSR F - Dead Sea Rift Fault; HG - Hammat Gader; LYG - Lower Yarmouk Gorge. **b** is modified after Sneh et al. (1998) and **c** (stratigraphic table) is modified after Fleischer (2002). The water source locations are listed in Appendix 1 and 2

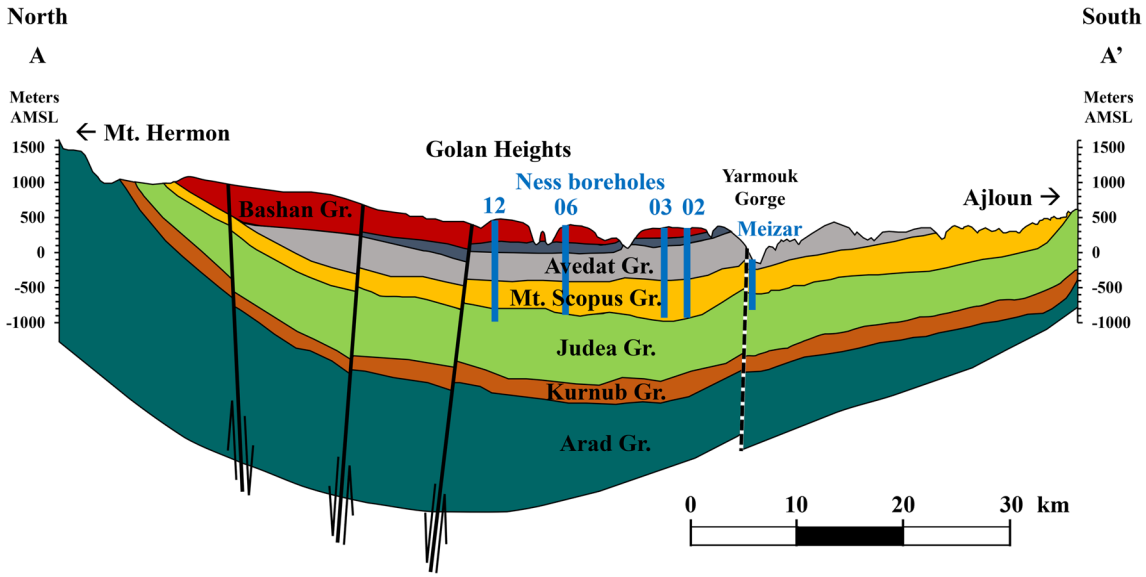

Fig. 2 Schematic cross section through the Golan Heights (GH) from Mt. Hermon in the north to the Ajloun anticline in the south—A–A′ in Fig. 1, after Burg and Gev (2019). Depths and locations of Ness and Meizar boreholes are indicated by light blue lines

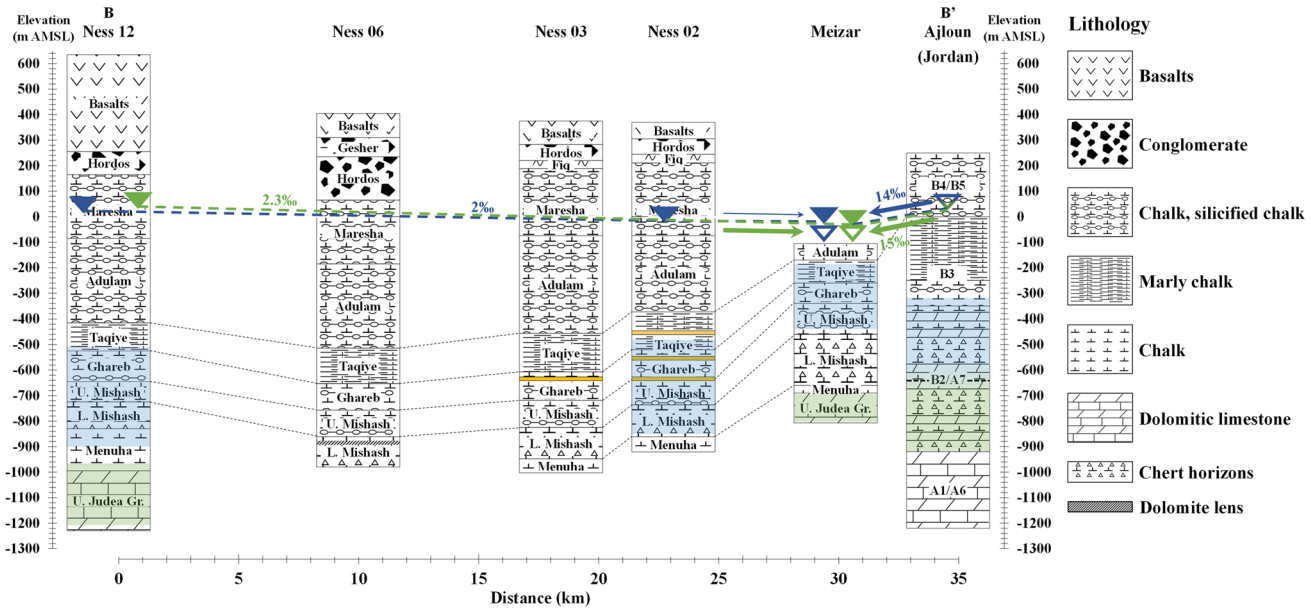

Fig. 3 Stratigraphic cross section through the studied boreholes in the GH including the Ajloun, northern Jordan (Fig. 1, B–B′). Depths of the drill stem tests (DSTs) are highlighted in orange. Open sections are highlighted in light blue for the Mt. Scopus Group and light green for the Judea Group. The same colors are used for water levels (triangles) and apparent hydraulic gradients (dashed line). Empty triangles mark the current water level in Meizar, which declined dramatically due to production at the LYG since its initial operation. According to the hydrogeological classification in Jordan, parts of the Mt. Scopus and the Judea groups are considered as one aquifer (A7/B2). The Ajloun stratigraphic section and water level (blue-green triangle) for the A7/B2 aquifer were compiled from Margane et al. (2002). Arrow thicknesses correspond with the relative contribution to Meizar wells, estimated by geochemical interpretation

Ma), known as the Cover Basalt (Heimann et al. 1996). In the northern GH and at the Yarmouk Gorge, younger basaltic flows that originated from local eruptions during the Pleistocene overlay the Cover Basalt (Mor 1993).

Hydrogeological background

The study area is located at the margins of two hydrogeological systems with the following main flow directions:

(1) The northern Golan Heights system that flows from the flanks of Mt. Hermon towards the Yarmouk (Arad and Bein 1986; Roded et al. 2013; Starinsky et al. 1979) and (2) The southern Ajloun system that flows from Ajloun to the Yarmouk (Bajjali et al. 1997; Margane et al. 2002).

The northern hydrological system of the GH includes two known and relatively well characterized regional aquifers: the Jurassic aquifer (Burg and Gev 2019) and the Basaltic aquifer (Dafny et al. 2003), which are recharged by direct precipitation through their respective outcrops (Fig. 1b). Other hydrogeological units (Kurnub, Judea, Mt. Scopus and Avedat groups) were not thoroughly studied. Further, these units were assumed to be hydrologically inactive mainly due to their limited outcrop area and/or low hydraulic conductivities (Roded et al. 2013; Tahal 1989).

The main southern hydrogeological systems are situated in the geological units that correlate to the Mt. Scopus and upper Judea groups—labeled B2 and A7, respectively, according to the Jordanian stratigraphic division (Margane et al. 2002; Siebert et al. 2014). These units are hydrogeologically active since they are widely exposed at the Ajloun anticline (Fig. 1b) and are readily available for direct recharge by precipitation (Margane et al. 2002), in contrast with the northern GH systems where the outcrops of these units are limited (Fig. 1).

In the LYG (Fig. 1b) the GH and Ajloun hydrogeological systems discharge through the thermal springs of Hammat Gader and Mukheiba (45.5 MCM year^{-1}, <50 °C; Levitte et al. 1978). In this area, a series of Jordanian and Israeli production wells (e.g., Meizar, Mukheiba and JRV) have produced water since the 1980s from these systems (Bajjali et al. 1997; Margane et al. 1999; Rosenthal et al. 2020). Previous geochemical and numerical modelling (Arad and Bein 1986; Starinsky et al. 1979) suggested the water in the LYG represents a mixture of the two hydrological systems (GH and Ajloun). However, the water composition flowing to the LYG from the GH and the contributing units remained unknown due to a lack of deep boreholes.

Materials and methods

Sample collection

Water samples from the Ness boreholes were collected using three principal methods with the first being high-pressure injection of air (airlift) from open-hole sections during drilling intermissions. The airlift samples were collected during the drilling operation of Ness 02 and 12 (Fig. 3). As these wells were drilled underbalanced using foam/air, drilling induced little contamination. Regardless, to avoid contamination, the accumulated water column in the wells was completely removed at least once prior to sampling. The second method was bottom hole samples (BHS) collected from specific depths, and the third comprised drill stem tests (DSTs) that targeted eight different 15-m intervals within the studied formations (Fig. 3).

Production of fluids during the DSTs was performed either by mechanical swabbing or by N_2 lift. The samples that were collected during the DSTs were closely monitored to ensure minimum contamination of drilling and completion fluids as much as possible. This was done by continuously monitoring the produced water using an electrical conductivity (EC) probe (WTW, 1970i) until a stable water composition (<5% change) was attained. From each tested zone, at least three representative samples were selected, each collected at slightly different times during the production. The representative samples selected from each zone were analyzed for detailed chemical analysis and their results were averaged. To avoid any remaining contamination by completion fluids that were used in the DSTs (predominantly KCl), in the relevant cases, the equivalent concentrations of K^+ were subtracted from the Cl^- concentrations: $[Cl^-]_{corrected}$ (meq) = $[Cl^-]$ (meq) – $[K^+]$ (meq) (all values are presented in Table 1).

Water levels and hydraulic conductivities

Water levels of open sections were measured during intermissions in the drilling operations of Ness 02 and Ness 12 wells (Fig. 3). The levels were measured following the complete removal of the fluids present in the well and a buildup period of 48 h to ensure the water level represents hydrostatic conditions. The apparent hydraulic conductivity of each DST interval was calculated using pressure transient analysis (PTA) of buildup periods (Satter et al. 2008), based on bottom hole pressure readings (Quartz, Spartek Systems).

Chemical and isotopic analyses

Major cations and sulfate (Na^+, K^+, Ca^{2+}, Mg^{2+}, Sr^{2+}, SO_4^{2-}) were measured by inductively coupled plasma optical emission spectrometry (ICP-OES, Optima 3300, Perkin Elmer, ±0.5%). The sum of Cl^- and Br^- was measured using automated potentiometric titration with $AgNO_3$ (702 SM Titrino, Methorn, ±0.5%). The concentration of Br^- was measured using ion chromatography (IC, ICS-200, Dionex, ±2%). Br^- concentration was subtracted from the sum to determine the Cl^- concentration ($[Cl^-] = [Cl^- + Br^-] - [Br^-] \pm 3\%$). Alkalinity was measured either by automatic titration (785 DMP Titrino, Methorn) or manually using a pH meter with a 0.05 N HCl acid for titration down to a pH of ~4.5. Stable oxygen (^{18}O) and hydrogen (^{2}H) isotopes were analyzed using an isotope ratio mass spectrometer—IRMS, Delta plus XP, Thermo Finnigan; $\delta^{18}O$ (±0.1‰) and $\delta^{2}H$ (±1.0‰)—and were corrected using

a Vienna Standard Mean Ocean Water (VSMOW) sample. Isotopic composition of Sr^{2+} was measured using a multicollector inductively coupled plasma mass spectrometer (MC-ICPMS, Nu Plasma-I, Wrexham, UK). The calibration standard that was used for correcting $^{87}Sr/^{86}Sr$ values was SRM-987 (55 ppb), $2\sigma \leq 1 \times 10^{-5}$. All analyses were performed at the Geological Survey of Israel (GSI) laboratories.

Results

Water levels and apparent hydraulic conductivities

Figure 3 presents borehole sections and water levels in the Mt. Scopus and Judea groups derived from the Ness wells in the GH, along with compiled literature data from Ajloun, Jordan. Open section water level values in Ness 12 and Ness 02 (Mt. Scopus Group) were 19 and –22 m above mean sea level (AMSL), respectively (Fig. 3). Water level of the Upper Judea Group in Ness 12 was slightly higher than the Mt. Scopus Group at the same well (24 m AMSL). Shortly after the Meizar 3 well (Mt. Scopus Group) was drilled (1984), the water level was 74.8 m above ground level (–30.2 m AMSL). The water level in the same well during sample collection (2016) was lower by more than 60 m, at –93.4 m AMSL. In Meizar 2 (Judea Group) the 1984 and 2016 artesian groundwater levels were –42.3 and –83.1 m AMSL, respectively (Simon et al. (1997) and Israel Hydrological Service). In Ajloun, both the Upper Judea (A7) and the Lower Mt. Scopus Groups (B2) are considered as one hydrogeological unit, which serves as the main water source in northern Jordan (Margane et al. 1999). The water levels in the A7/B2 aquifer, 4 km southward of the LYG (Fig. 1b) are ~25 m AMSL (Fig. 3; Margane et al. 2002).

Apparent hydraulic conductivities calculated from the DSTs were the same (2×10^{-7} m/s) for all intervals that included the Ghareb-Upper Mishash formations (GUMF). However, the overlying Taqiye Formation exhibited a hydraulic conductivity that was lower by two orders of magnitude (2×10^{-9} m/s). Values and depths are detailed in Appendix 1.

Geochemical composition

The salinities of the analyzed samples varied spatially, spanning over three orders of magnitude between different locations and depths in the Mt. Scopus Group (Table 1). Water collected from the Mt. Scopus Group in Ness 12 was fresh (<420 mg/L total dissolved solids, TDS). Similarly, the water collected from the Upper Judea Group in the same well was fresh (<700 mg/L TDS). The water collected during the DSTs in the Upper-Mishash and the Ghareb formations (GUMF) in Ness 02 and Ness 03 was moderately saline (5,000–6,300 mg/L TDS) and the water from the Taqiye Formation in Ness 02 was saline (~17,000 mg/L TDS). Water from the open section in Ness 02 (Fig. 3), which includes all the tested formations during the DST and additional contributing layers, was considerably less saline (2,800 mg/L TDS) than the DST samples in the same well (5,000–6,300 mg/L TDS).

Despite the range in salinities, the brackish to moderately saline water from the tested DST intervals had similar equivalent ratios (Table 2). Na/Cl ratios were lower than the marine value (<0.86). Mg/Ca ratios were low and with limited variation (0.2–0.3), and all samples exhibited a Ca-chloride composition. In contrast, the less saline water collected from the open sections in both Ness 12 (fresh) and Ness 02 (brackish) had higher Na/Cl (0.9–1.5) and Mg/Ca (0.7–0.9) ratios and was not Ca-chloride (Table 2). The electrical charge balance in all the samples that were analyzed did not exceed ±3%.

Isotopic composition

The $\delta^{18}O$ and $\delta^{2}H$ (VSMOW) of the studied water are presented in Table 2. Freshwater samples from both the Mt. Scopus and Upper Judea groups in Ness 12 showed depleted $\delta^{18}O$ and $\delta^{2}H$ values (≤ -7.3 and $< -42‰$, respectively). Brackish-moderately saline water from the Mt. Scopus Group in Ness 02 and Ness 03 had slightly less depleted $\delta^{18}O$ and $\delta^{2}H$ values (≤ -7 and $< -40‰$, respectively). Saline water from the Taqiye Formation in Ness 02 had significantly higher $\delta^{18}O$ and $\delta^{2}H$ values of –6 and –36‰, respectively.

$^{87}Sr/^{86}Sr$ values of the studied water from the southern wells (Ness 02 and 03) were mostly similar (Table 2). $^{87}Sr/^{86}Sr$ values of the water from the Mt. Scopus Group were 0.70766–0.70782. The freshwater from the northern well (Ness 12) had significantly lower $^{87}Sr/^{86}Sr$ values (0.70746 in the Mt. Scopus Group and 0.70737 in the Judea Group).

Discussion

Regional hydraulic gradients

Calculation of preproduction hydraulic gradients based on the water level measurements highlight the differences between the southward flowing GH and northern flowing Ajloun systems: firstly, in the GH, the gradients from Ness 12 to Meizar in the Mt. Scopus and Judea groups are moderate (1.7 and 2.3‰, respectively). Despite the similar gradients, the water levels in the Mt. Scopus and Judea groups in both the Ness 12 and Meizar wells are different, indicating that the water systems are isolated. Secondly, in the

Table 1 General information regarding the samples and ion concentrations in the studied water. *Corr. Cl^-* is the Cl^- concentration after subtraction of the equivalent K^+ concentration (see section 'Sample collection'). Depths and locations are detailed in Appendix 1. *DST* - drill stem test. *TDS* - total dissolved solids

Borehole	Formation	Sampling method	Sampling date	pH	Concentration (mg/L)										
					Na^+	K^+	Ca^{2+}	Mg^{2+}	Sr^{2+}	Cl^-	Corr. Cl^-	Br^-	SO_4^{2-}	HCO_3^-	TDS
Ness 02	Ghareb-Upper Mishash boundary	DST- avg. of three samples	26/04/2016	6.7	824	422	757	87.0	18.2	2,921	2,538	10.5	31.9	479	5,391
Ness 02	Ghareb	DST- avg. of four samples	10/05/2016	6.3	903	553	433	68.6	12.9	2,451	1,950	23.7	51.9	607	5,090
Ness 03	Ghareb	DST- avg. of three samples	18/03/2016	6.7	1,189	341	784	85.0	22.4	3,433	3,123	18.6	28.6	552	6,270
Ness 02	Taqiye	DST- avg. of three samples	19/05/2016	7.3	4,489	163	1271	169	43.4	9,967	-	55.7	40.2	548	16,746
Ness 02	Lower Taqiye-Lower Mishash	Airlift	02/07/2016	8.3	717	46.0	101	53.0	8.80	1,240	-	8.10	7.00	565	2,746
Ness 12	Lower Taqiye-Lower Mishash	Airlift	21/12/2015	8.1	76.0	8.00	27.0	14.0	1.28	90.0	-	0.50	13.0	187	417
Ness 12	Upper Judea Gr (Bina-Dir Hana)	Airlift and BHS- avg. of five samples	March–May 2020	8.0	109	13.0	59.5	24.5	2.27	110	-	-	179	190	687

Table 2 Ion equivalent ratios and the isotopic composition and ratios in the studied water

Borehole	Formation	Equivalent ratios					$\delta^{18}O$ (‰ VSMOW)	$\delta^{2}H$ (‰ VSMOW)	d-excess (‰)	$^{87}Sr/^{86}Sr$
		Na/Cl	Mg/Ca	Mg/Cl	Ca/Cl	$Ca/(HCO_3 + SO_4)$				
Ness 02	Ghareb-Upper Mishash boundary	0.50	0.19	0.10	0.53	4.70	–7.45	–40.7	18.9	0.70773
Ness 02	Ghareb	0.71	0.26	0.10	0.40	2.24	–7.24	–41.0	17.0	0.70773
Ness 03	Ghareb	0.59	0.18	0.08	0.44	4.04	–6.99	–42.1	13.8	0.70766
Ness 02	Taqiye	0.69	0.22	0.05	0.23	6.48	–6.01	–36.3	11.8	0.70782
Ness 02	Lower Taqiye-Lower Mishash	0.89	0.87	0.12	0.14	0.54	–7.20	–42.4	15.2	0.70784
Ness 12	Lower Taqiye-Lower Mishash	1.30	0.86	0.45	0.53	0.40	–7.26	–42.0	16.0	0.70746
Ness 12	Upper Judea Group (Bina-Dir Hana)	1.53	0.68	-	0.96	0.43	–7.47	–44.40	15.4	0.70737

Ajloun system, where the Mt. Scopus and Judea groups are considered hydraulically connected (Margane et al. 2002) significantly steeper gradients were calculated towards the Meizar wells (14‰ in Mt. Scopus Group towards Meizar 3 and 17‰ in the Judea Group towards Meizar 2).

Following the intensive water production that took place in the Meizar wells in the past 40 years, the hydraulic gradients towards the Meizar wells have steepened to ~10 and 30% for the GH and Ajloun systems, respectively. Assuming that similar hydraulic conductivities are present north and south of the Yarmuk, the significant gradient differences (either pre- or post-production) suggest faster natural flow rates from the Ajloun system compared to the GH system.

Chemical composition and sources of salinity

The Cl^- concentrations in the water from the DSTs performed in Ness 02 and Ness 03 wells (Fig. 1b) are between 2,400 and 10,000 mg/L. The highest Cl^- concentration was found in the water from the Taqiye Formation (~10,000 mg/L), which is also higher than any concentration previously recorded in GH groundwater. Along with high Cl^- concentrations, brackish-saline water in the Mt. Scopus Group exhibits Na/Cl and Mg/Ca equivalent ionic ratios that are lower than the marine values with a Ca-chloride composition (Table 2). While remnants of seawater can explain such salinities, the ionic ratios of the samples are not similar to those of seawater (Fig. 5). Further, water–rock interactions between meteoric water and host rock cannot explain the high Na^+ and Cl^- concentrations. Halite dissolution which could increase the Na^+ and Cl^- concentrations is also overruled as this would have resulted in Na/Cl values of 1 (Carpenter 1978; Kreitler 1989). Therefore, the composition of the studied water cannot be explained without an additional salinity source that formed separately from the host rock in which it is found today.

Waters with Ca-chloride compositions are abundant along the Dead Sea Rift (DSR) Valley, including the modern Dead Sea as well as in ancient brines that intruded groundwater systems around the rift. This includes the subsurface surrounding Lake Kinneret (Klein-BenDavid et al. 2004; Mazor and Mero 1969; Starinsky and Katz 2014) where Ca-chloride saline waters (termed as the Kinneret brines) are found also with Cl^- concentrations in the range of 1,000–25,000 mg/L and low Na/Cl ratios. Furthermore, a few kilometers north of Lake Kinneret, a hypersaline water body was found in the Rosh Pina-1 well (Fig. 1b) with a Cl^- concentration of more than 100,000 mg/L. The Kinneret brines and Rosh Pina Brine (RPB) were previously defined as remnants of the DSR brines (Starinsky 1974; Starinsky and Katz 2014).

The DSR brines evolved from seawater that transgressed during the Neogene through Yizra'el Valley (Fig. 4a) into the tectonic depression that formed along the DSR to form a lagoon (Lagoonary stage; Neev 1967; Zak 1997; Zak and Bentor 1972). The seawater underwent evaporation which led to an increase in salinity and to the precipitation of aragonite, gypsum and halite (decrease in Na/Cl and increase in Mg/Ca). The increase in salinity was accompanied by an increase in density which resulted in a density-driven migration into the surrounding rocks (Stanislavsky and Gvirtzman 1999).

Following the intrusion, at the subsurface, the brines interacted with carbonates to form dolomite. The dolomitization process increased Ca^{2+} concentrations, which led to gypsum precipitation and a subsequent decrease in SO_4^{2-} concentrations. The combination between the dolomitization and mineral precipitation resulted in a decrease in Mg/Ca and increase in $Ca^{2+}/(HCO_3^- + SO_4^{2-})$, which led to the Ca-chloride composition. Lagoon level drops led to the backflow of previously intruded brines while gradually decreasing the Mg/Ca ratio. Following the terminal disconnection of the lagoon from the sea (lacustrine stage; Neev 1967; Stein 2014), inflow of bicarbonate-rich freshwater led to aragonite precipitation (increase in Mg/Ca). The geochemical evolution of the DSR brines enabled division of the saline water found in the DSR into two groups (Katz and Starinsky 2009): (1) brines from the lagoonary stage, with Mg/Ca ratios lower than 1, and (2) brines from the lacustrine stage, with Mg/Ca higher than 1 (Fig. 4b).

In the south of Israel, brines from the earlier lagoonary stage were found at a distance of up to 90 km from the rift, while brines from the later lacustrine stage were only found within the DSR (Fig. 4a; Katz and Starinsky 2009; Stein 2001). In northern Israel, lagoonary brines are found in springs west of Lake Kinneret, while lacustrine brines are found east of Lake Kinneret in the shallow alluvial basin fill units (Fig. 4a, empty purple triangle). The RPB hypersaline brine was found in the research well Rosh Pina-1, located in the Hula Valley, north of Kinneret Lake. The RBP was found at a depth of 3,800 m in Jurassic limestones. The limestones in which the RPB was found are a part of a block within the DSR, which is separated from its surroundings by deep faults (Heimann and Ron 1993).

To examine the relationship between the studied water from the southern GH and surrounding saline water sources, cation concentrations were plotted vs. Cl^- concentration (Fig. 5a–e). Detailed chemical compositions are presented in Appendix 2. Also plotted, are RPB-freshwater and seawater–freshwater mixing lines. The freshwater end-member composition selected is the water found upstream in Ness 12. Note that due to extreme salinity differences between hypersaline brines and freshwater, even significant

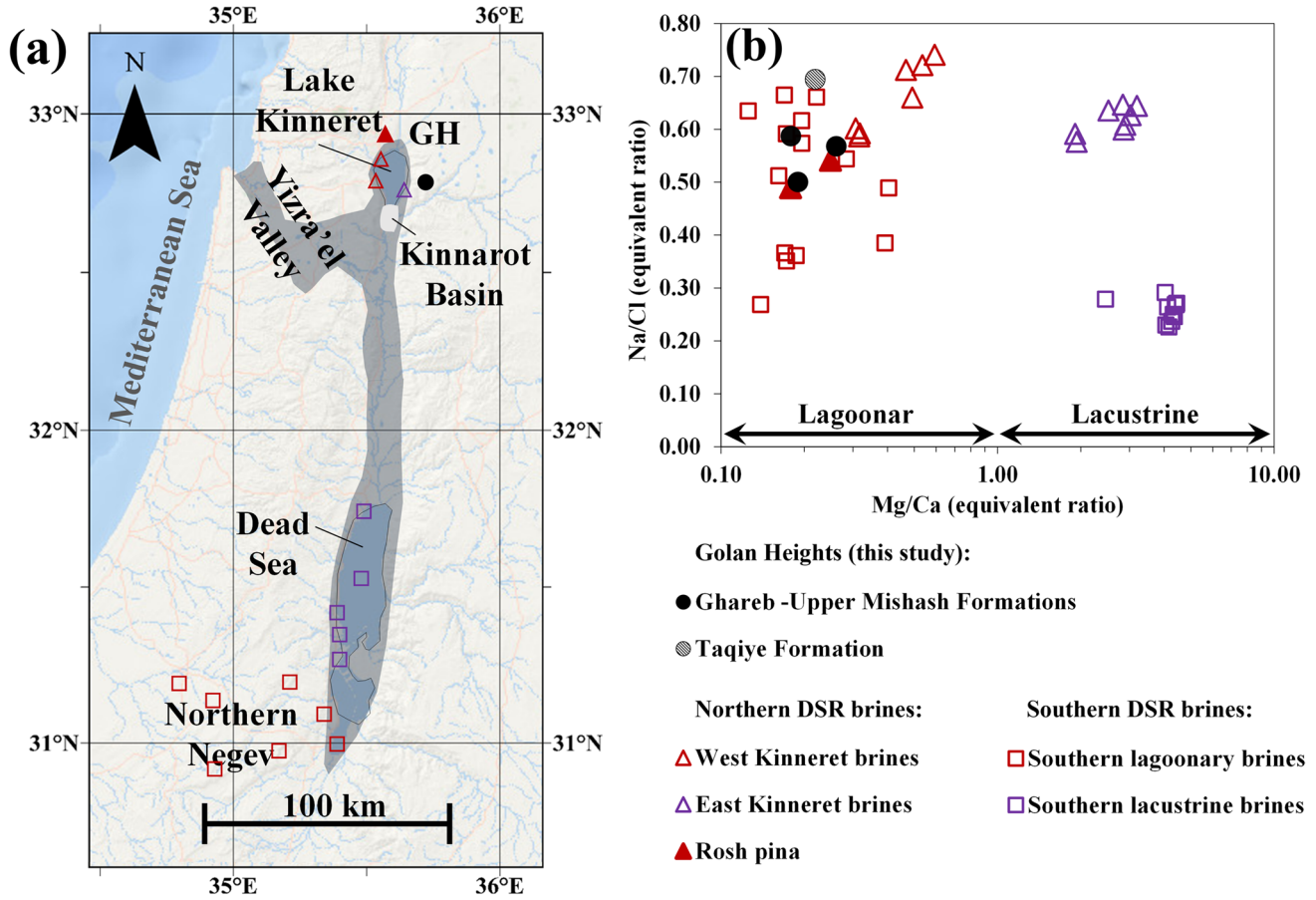

Fig. 4 **a** Distribution of marine transgression according to evaporitic deposits (gray polygon) and intruding DSR brines found at the subsurface surrounding the rift (lagoonary and lacustrine brines in red and purple, respectively; modified after Zak and Bentor 1972); **b** Na/Cl vs. Mg/Ca of the DSR brines and the studied water (modified after Starinsky and Katz 2014). GH water chemical compositions are detailed in section 'Geochemical composition' (Tables 1 and 2). DSR brine compositions were reported in Bergelson et al. (1999) and Starinsky and Katz (2014). The compositions are detailed in Appendix 2

brine dilution (>1% brine fraction) has little effect on the ionic ratios of the brines, thereby preserving the original ionic ratios of the ancient brines. Figure 5 indicates that the water found in the GUMF formation in the GH shares a common salinity source as the RPB. This means that a DSR brine with similar composition to the RPB intruded the GH subsurface.

Assuming that the RPB represents the closest brine composition to the brine that intruded the GH, the residual fraction of the hypersaline endmember can be calculated. Calculation of the RPB fraction based on Na^+, Ca^{2+}, Mg^{2+} and Cl^- suggest that the water from the GUMF retains 2–3% of the saline fraction, while the remaining 97% are freshwater that diluted and flushed the original brine. The Na/Cl ratios in the water from the Taqiye Formation are slightly different from those in the GUMF, suggesting that the composition of the hypersaline brine that intruded it was slightly different. Thus, when taking the RPB as the hypersaline end member, the calculated volume fractions in the Taqiye have a larger scatter: based on Na^+ and Cl^-, the Taqiye contains 10–13% brine (with a composition of the RPB) and only 5–6% based on the Mg^{2+} and Ca^{2+} concentrations. The higher dilution degrees in the GUMF in comparison to the Taqiye Formation demonstrates the separation between the two units as well as their different hydraulic characteristics—i.e., less dilution is exhibited in the less-permeable Taqiye compared to the GUMF. Nevertheless, it should be noted that, despite the two orders of magnitude difference in the formation hydraulic conductivities, the saline endmember in the Taqiye has also been significantly diluted by freshwater (more than 87%).

Source of freshwater

In contrast with the dissolved ions that are mostly affected by the hypersaline brine endmember, the isotopic signal of the studied water should be governed by the freshwater component, as the samples are significantly diluted.

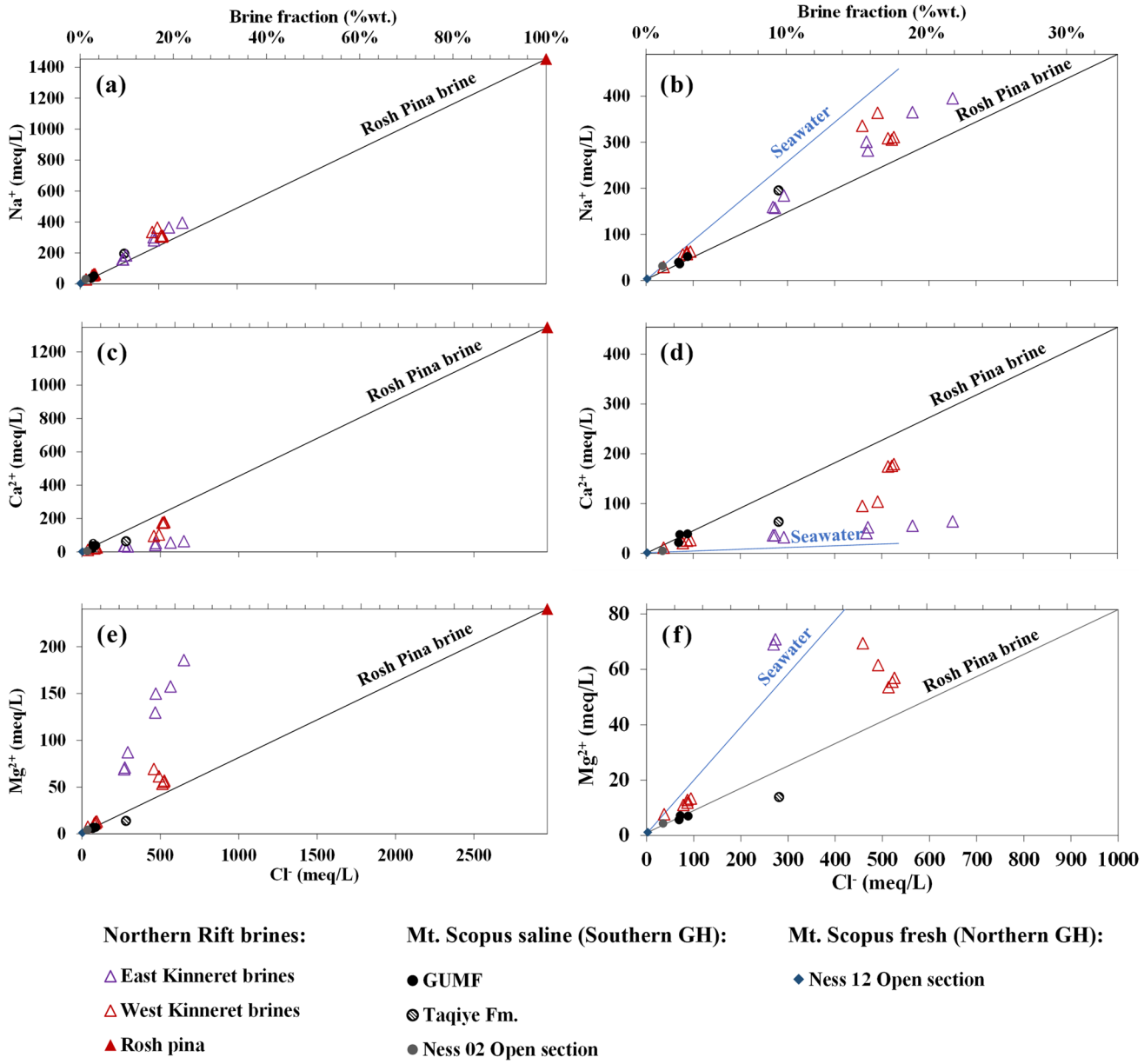

Fig. 5 Major cations vs. Cl^- equivalent concentrations for both the studied water and nearby saline water bodies in the GH region. Subplots in the right panel are enlargements of the subplots in the left panel. Theoretical mixing lines between freshwater and Rosh Pina Brine (RPB) were added. Additional mixing lines with seawater were added to the subplots in the right panel for comparison. The brine fraction (upper horizontal axis) was calculated based on the Cl^- concentration. The lagoonary brines west of the Kinneret show slight compositional differences compared to the RPB mixing line, while the lacustrine brines east of the Kinneret exhibit a completely different end-member composition, as also shown in Fig. 4. DSR brine compositions were reported in Bergelson et al. (1999) and Starinsky and Katz (2014). The compositions are detailed in Appendix 2

The $\delta^{18}O$ of the freshest and most upstream water sample is –7.3‰ (Ness 12, Fig. 1b). This value is similar to the $\delta^{18}O$ values found in the deep aquifers that are recharged in Mt. Hermon and its elevated vicinity (Dafny et al. 2006; Kattan 1997). In contrast, the $\delta^{18}O$ value of RPB is +3‰ (Gat et al. 1969), i.e. particularly enriched and indicative of water that underwent significant evaporation. Figure 6a presents the $\delta^{18}O$ values vs. Cl^- concentrations of the studied water with a mixing line between the RPB and the freshwater found in Ness 12. The results show that the $\delta^{18}O$ values of the water samples fall on the suggested mixing line, exhibiting increasing $\delta^{18}O$ values with increasing salinity. Most notably, the least diluted water from the Taqiye Formation exhibit the highest $\delta^{18}O$ values (–6.0‰),

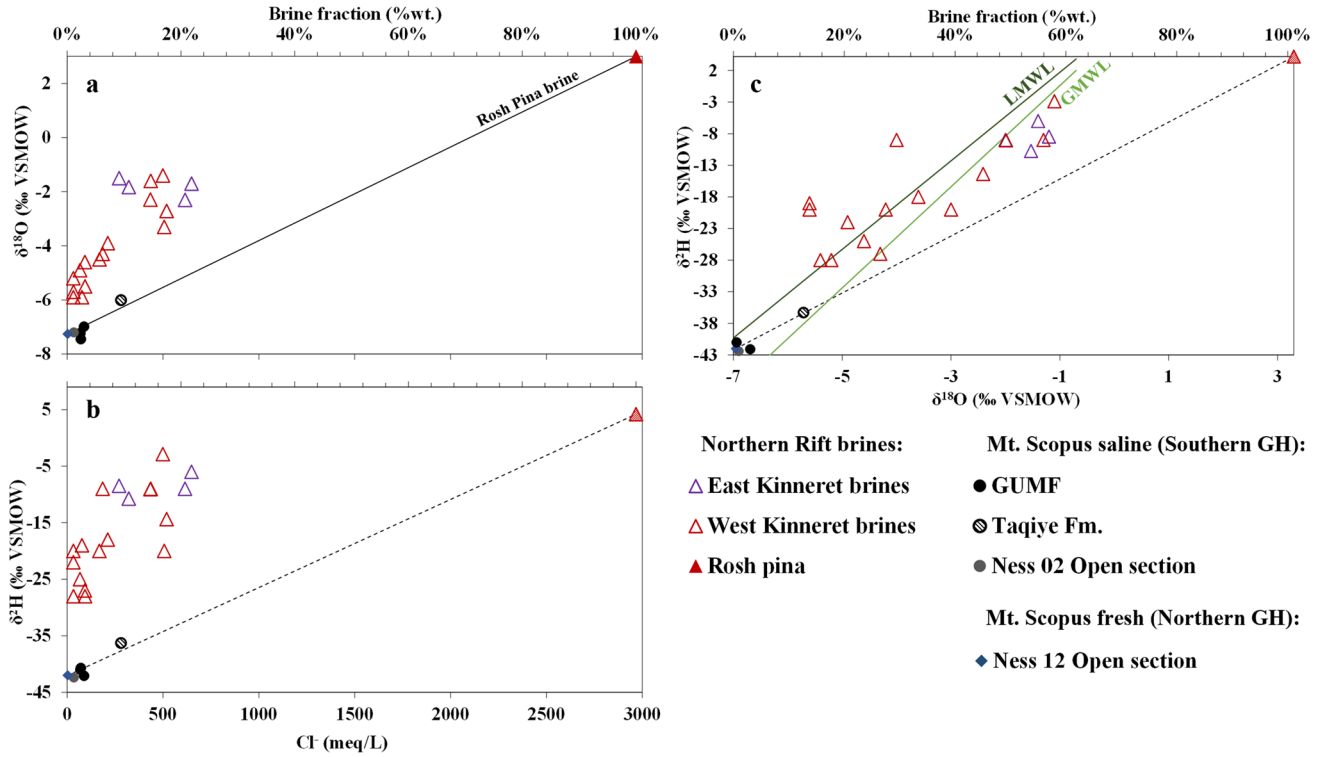

Fig. 6 **a** $\delta^{18}O$ and **b** $\delta^{2}H$ values vs. Cl^{-} concentrations in the studied water and nearby water bodies. **c** $\delta^{2}H$ vs. $\delta^{18}O$ values with global and local meteoric water lines (GMWL and LMWL, respectively). LMWL is based on Mt. Hermon and Syria precipitation values after Al Charideh and Abou Zakhem (2010). Also plotted are the mixing lines (black) between the Mt. Scopus Group freshwater endmember and RPB, where dashed lines are mixing lines with estimated $\delta^{2}H$ value of the saline endmember. The brine fraction (upper horizontal axis) was calculated based on the Cl^{-} concentrations. Cl^{-} concentrations, $\delta^{2}H$ and $\delta^{18}O$ of the northern DSR brines (triangles) were taken from Gat et al. (1969) and are fully detailed in Appendix 3

as it is slightly more affected by the heavier isotopic composition of the saline endmember.

Similarly, Fig. 6b presents $\delta^{2}H$ values vs. Cl^{-} concentrations of the studied water with a mixing line between the hypersaline and the freshwater endmembers (Ness 12, –42‰). Since the $\delta^{2}H$ value of the RPB was not measured, the value was assumed to be +4.2‰, in accordance with the linear relationship between $\delta^{18}O$ and $\delta^{2}H$ found in the Dead Sea brine (Horita and Gat 1989). The $\delta^{2}H$ values of the studied water also increase with salinity and conform with the mixing line, which reinforces the conclusion drawn based on $\delta^{18}O$.

The calculated RPB volume fraction, based on the mixing lines of both $\delta^{18}O$ and $\delta^{2}H$, yielded a value of 12% in the water from the Taqiye Formation, which falls within the range defined by the dissolved ions (Na^{+} and Cl^{-}, 10–13%). Likewise, the brine volume fraction in the water from the GUMF was less than 3% (based on both $\delta^{18}O$ and $\delta^{2}H$), which matched the mixing ratios derived based on the dissolved ions (2–3%). Thus, the isotopic compositions of the water further support the two end-member mixing model for the studied water in the Ness wells. It should further be noted that in contrast with the studied water in the GH, the Kinneret brines exhibit more enriched $\delta^{18}O$ and $\delta^{2}H$ compositions, indicating they were diluted by different freshwater sources (Fig. 6).

The isotopic composition of the freshwater endmember is very light (–7.3 and –42‰ for $\delta^{18}O$ and $\delta^{2}H$, respectively). The closest such depleted isotopic compositions are found in rainwater that precipitate over elevations higher than 1,000 m AMSL, such as Mt. Hermon and its foothills (Fig. 1b), or the distant Palmyride Mountains (Dafny et al. 2006; Kattan 1997). The depleted $\delta^{2}H$ values of the studied water (~ –42‰), resemble the values on the southern flanks of the Hermon Mt. (< –40‰) and suggests the source of the freshwater is probably not from the distant slopes of the Palmyride Mountains, where $\delta^{2}H$ values are more enriched (> –35‰) (Kattan 2021). The northern water source also conforms with the north–south modern regional hydraulic gradient found in the present study for the Mt. Scopus and Judea groups in the southern GH (Fig. 3). This also suggests that the dilution and flushing process is ongoing and

therefore the light isotopic composition and brine remnants should be detected downstream.

Lower Yarmouk Gorge outlets: water and salinity sources

The gradient and chemical and isotopic composition suggest that the Mt. Scopus and Judea groups are not inactive, as previously suggested, and may potentially serve as one of the contributing units to the LYG outlets. The salinities of the LYG springs are relatively low, yet their chemical composition suggests that their salinity source relates to the lagoonary stage of the DSR brines (Starinsky et al. 1979). To investigate the relationship between the northern GH systems, the southern Ajloun system and wells and springs located downstream, such as the Meizar wells and LYG spring outlets, the compositions of different water sources in the area were compiled and analyzed (Fig. 7).

Figure 7a shows high Na/Cl values in the freshwater samples that are not affected by the brine composition. With increasing salinity, however, the Na/Cl ratios decrease below the marine value due to a higher volume fraction of DSR brines remnants. The decrease in Na/Cl values with increasing salinity indicates that the source of salts in both the GH and the downstream LYG has a lower Na/Cl value (Fig. 7a). The isotopic composition shows two distinctly different freshwater sources: the relatively saline and isotopically light GH component and the fresh and isotopically heavier Ajloun component (–5 to –6.5‰; Bajjali et al. 1997). The data of the LYG fall within a range defined by the Ajloun component and the GH component, which by itself is a mixing product of hypersaline brine and isotopically light freshwater. This mixing explains the increase in salinity with decreasing $\delta^{18}O$ values observed in the LYG water (Fig. 7b, orange lines).

Based on this mixing pattern, the water in the Mt. Scopus Group in Meitzar 3 is mainly derived from the south (relatively enriched $\delta^{18}O$ and low salinity; Fig. 7b, dark blue square), which is typical for rainwater that precipitated on outcrops of the Mt. Scopus Group at the Ajloun slopes. In contrast, the isotopic composition in the underlying Judea Group in Meitzar 2 indicate that the water is mainly derived from the GH system (depleted $\delta^{18}O$ and relatively higher salinity; Fig. 7b, green squares).

$^{87}Sr/^{86}Sr$ values add additional information regarding the source of the salt and the host rock the water interacted with. The isotopic $^{87}Sr/^{86}Sr$ signature of the freshwater is largely acquired by water–rock interactions (Kendall and Doctor 2003) with the latter having the seawater composition at the time that they precipitated (Burke et al. 1982). However, when the isotopic signal of the water and the host rock differ significantly–the difference can be explained by an additional source of Sr, such as remnants of brine (Chaudhuri and Clauer 1993). In the case of the studied water from the GH, only the freshwater samples are congruent with the host rocks (Fig. 7c, Ness 12 and Meitzar 03). The rest of the brackish-saline samples (Ness 03, 02, Meitzar 02, LYG springs) show higher $^{87}Sr/^{86}Sr$ isotopic values (0.7077–0.7079) with respect to the values of the Late Cretaceous rocks (0.7073–0.7077) (Burke et al. 1982; McArthur et al. 1994), excluding the data point of the Ghareb Formation in Ness 03 that falls slightly out of range. This is evident in both the Mt. Scopus Group and Judea Group waters that show a prominent increase in $^{87}Sr/^{86}Sr$ along the flow path from Ness 12 (Fig. 7c). The increase in $^{87}Sr/^{86}Sr$ is explained by the presence of lagoonary brines, with values as high as 0.708 (Starinsky and Katz 2014). Similarly to the $\delta^{18}O$ mixing lines (Fig. 7c), the $^{87}Sr/^{86}Sr$ values of the water samples as a function of salinity can be explained by mixing an enriched lagoonary brine with freshwater that inherited the $^{87}Sr/^{86}Sr$ values of the Mt. Scopus and Judea rocks (Fig. 7c).

In summary, based on Na/Cl and $^{87}Sr/^{86}Sr$, the salinity sources of the GH and Yarmouk are similar, while the $\delta^{18}O$ distinguishes between the freshwater sources of the GH and Ajloun. The water found in both Meitzar 2 and LYG springs was shown to be geochemically related to the northern component that contains brine remnants. Therefore, it is concluded that flushing of the remaining DSR brine from the Mt. Scopus and Judea groups in the GH, and possibly from other units as well, still continues today through discharge in the LYG springs.

Paleo-hydrological reconstruction

During the past 9.5 Ma, significant tectonic and basin changes have occurred in the area due to the dextral displacement along the Dead Sea transform. The overall movement during the last 25 Ma is estimated at 35–40 km (Freund et al. 1968; Walley 1998), which would have placed the Ness boreholes several kilometers closer to the Kinnarot basin prior to the movement (Fig. 8a). This tectonic movement also resulted in the uplift of the Hermon Mountain ridge (Garfunkel 1981; Heimann et al. 1990) which initiated the freshwater hydrogeological system sourced in the north.

Given the foregoing, a conceptual model demonstrating the intrusion of the hypersaline brine to the subsurface and their subsequent dilution and flow reversal, due to the major tectonic shifts over time, is presented

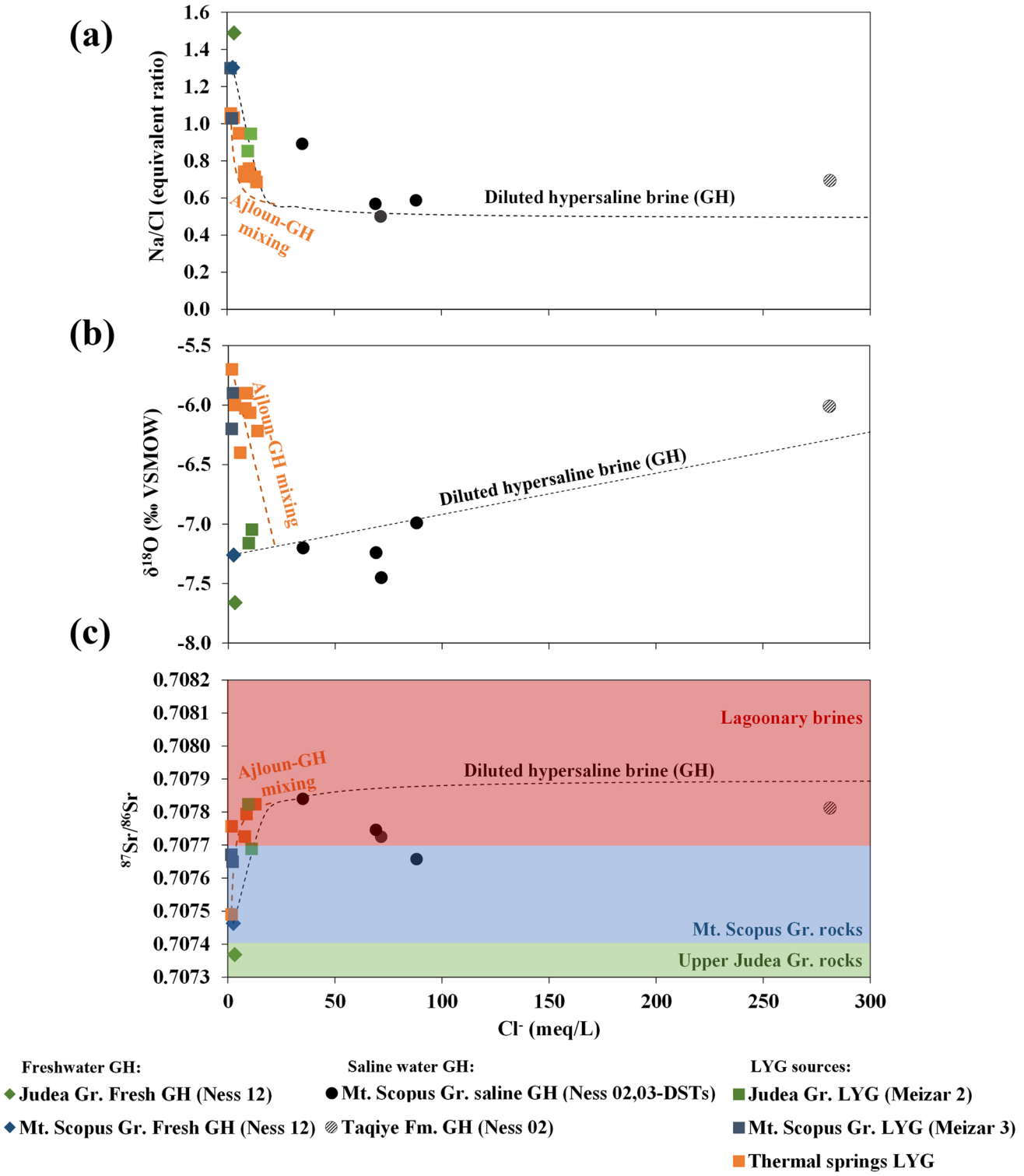

Fig. 7 **a** Na/Cl equivalent ratio, **b** $\delta^{18}O$ and **c** $^{87}Sr/^{86}Sr$ vs. Cl^- concentrations of the studied water of Golan Heights (GH). Mixing lines were added to show the change in geochemical properties as a function of salinity. $^{87}Sr/^{86}Sr$ values of the northern lagoonary brines were taken from Starinsky and Katz (2014) (0.7077–0.708). $^{87}Sr/^{86}Sr$ values of the Mt. Scopus and Judea Groups rocks are from McArthur et al. (1994). The chemical and isotopic compositions of the LYG water were taken from previous publications (Bajjali et al. 1997; Gavrieli and Burg 2002), as well as analysis performed by the Israel National Water Co. (Mekorot Co.). All compositions are detailed in Appendix 3 and 4

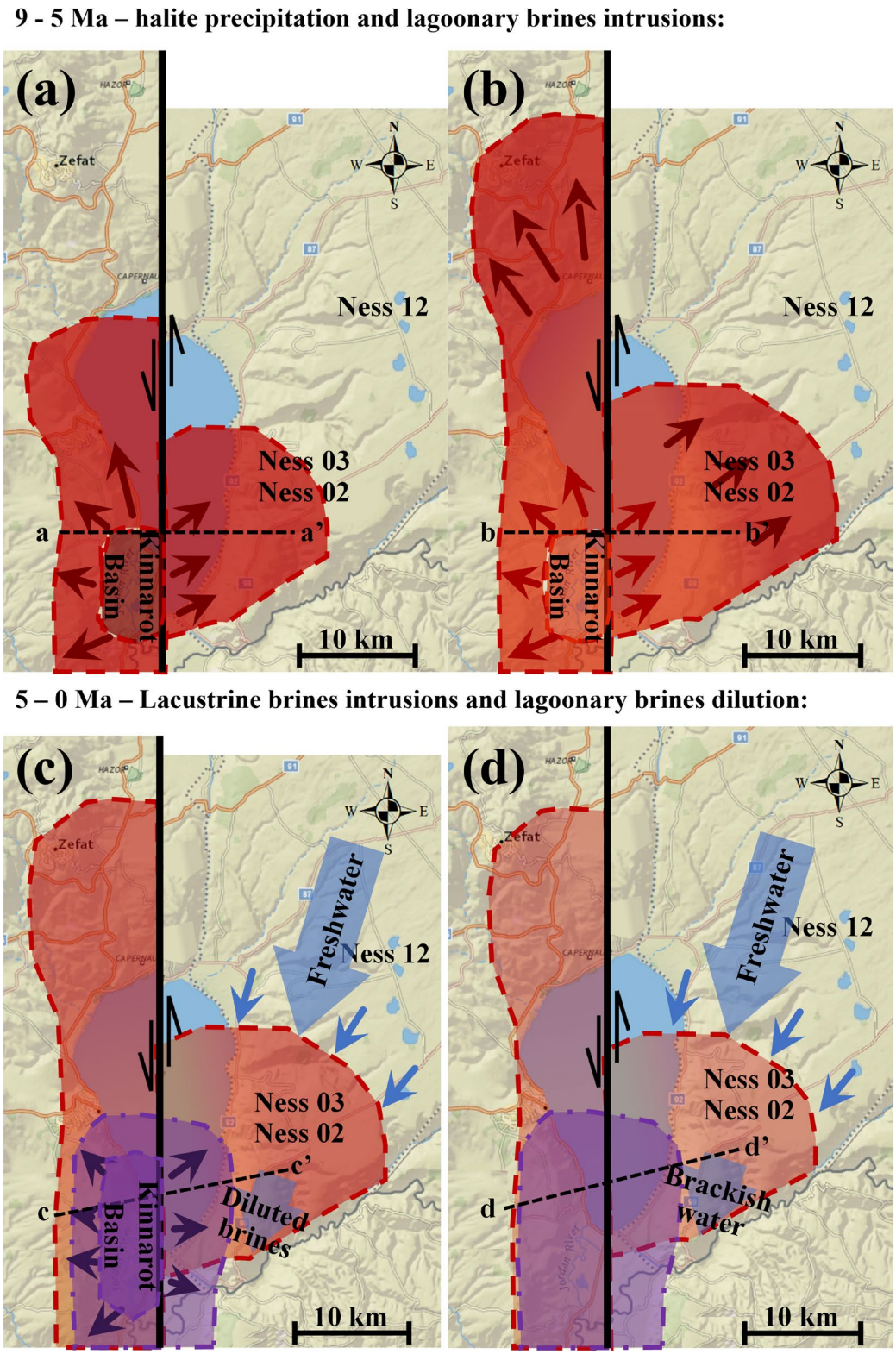

Fig. 8 A conceptual model demonstrating the intrusion and flushing of the northern DSR brines. The intrusion of the lagoonary brines to the subsurface occurred concurrently with the precipitation of halite in the Kinnarot basin (**a**–**b**, red). The brines' ongoing migration created spatial chemical composition differences. Subsequently, lacustrine brines that were formed after the disconnection from the Mediterranean Sea intruded into shallow units inside and nearby the DSR (**c**, purple). Following the intrusion, freshwater activity led flow reversal, dilution and flushing of the lagoonary brines (increasingly lighter red) into the natural outlets along the LYG (**d**). Dashed lines mark the locations of the cross sections in Appendix 5

in Fig. 8. Initially, during the Neogene, seawater transgressed (Fig. 4a) into a tectonic depression that developed along the DSR and formed a semiclosed lagoon (lagoonary stage). The seawater underwent intensive evaporation which led to an increase in solution density and salinity, and to precipitation of evaporites (predominantly halite). Concurrently, several pull-apart basins developed along the Dead Sea Rift and provided sufficient accommodation space for the halite to accumulate through rapid subsidence. The subsidence enabled the deposition of massive evaporite bodies near Lake Kinneret within the Kinnarot basin, where 900 m of halite were deposited across a 2.5-km section of alternating magmatic and sedimentary beds (Marcus and Slager 1985; Rozenbaum et al. 2019).

For halite to precipitate from seawater, a degree of evaporation of tenfold and above is required. At such degrees of evaporation, the density of the evaporated seawater is higher by >20% relative to freshwater. The elevated density increases the hydraulic head within the basin compared to the surrounding hydrogeological systems, which can result in the necessary driving force for the intrusion of the brines to the surrounding rocks (density-driven migration) while displacing freshwater (Stanislavsky and Gvirtzman 1999). In the subsurface, the brines can migrate over long distances (tens of kilometers) assuming no hydraulic barriers (Stanislavsky and Gvirtzman 1999). The fact that no brines were found northwards of Ness 03 suggests that the intrusion may have been restricted by the rising water head which is due to the elevated geological structure towards the Hermon Mountain range (Fig. 2).

Ar–Ar ages of basaltic flows from the top and base of the halite deposits in the Kinnarot Basin provide a general time constraint of ~9.5–5 Ma for the deposition of the halite sequence (Stein 2014). Based on the dating results, a similar time interval was defined as the geological period of the lagoonary brines formation and intrusion (Fig. 8a–b, red–orange). During this time window, dilution/evaporation cycles occurred in the lagoon (Raab et al. 1997; Rozenbaum et al. 2019), which could have led to numerous intrusion events of brines with different densities and chemical compositions.

During the subsequent lacustrine stage that followed the lagoonary stage (5 Ma to present), the basin disconnected from the sea. During this period, hypersaline lake water was significantly diluted by freshwater and halite stopped to precipitate in the Kinnarot basin. These diluted lacustrine brines are found only in shallower units within the DSR, likely due to their lower density compared to the lagoonary brines (Fig. 8c, purple).

Over time, active fresh groundwater flow led to gradual subsurface dilution of the brines. In order for the brines to be flushed out of a given hydrogeological unit, the freshwater system has to exhibit a driving force that can overcome the high density of the brine.

With the lack of a driving force, brines will remain stagnant over geological periods. Elevated recharge areas were shown to create a topography-driven force that can gradually flush brines from deep sedimentary units (Ferguson et al. 2018). The extent of dilution depends on the recharge rate of the freshwater component and the hydraulic conductivity of each unit.

The high altitude of the Hermon range in the north (Fig. 1b) provides the necessary driving force for the flow and flushing to take place and overcome the high density of the brines. The brines that were flushed by freshwater discharged through the natural outlets in the LYG, while gradually decreasing the salinity of the water (Fig. 8d).

Conclusions

The water compositions found in the deep hydrogeological systems in the southern Golan Heights (GH) allowed for reconstruction of the unique paleo-hydrogeological setting of the area. The Upper Cretaceous rocks from the Mt. Scopus and Judea groups were shown to contain remnants of ancient Ca-chloride lagoonary Dead Sea Rift (DSR) brines, estimated to have formed 10–5 Ma ago in a subsiding basin within the DSR, where a massive halite section was deposited.

The intrusion process was controlled by lake level and density on one hand, and the groundwater level elevations in the surrounding hydrogeological systems on the other. The combination of all these processes resulted in intrusion/backflow where some of the brines that were chemically modified by water–rock interactions back-flowed into the rift. These dynamics have led to compositional differences in area as well as in different geological units.

Following the intrusion to the subsurface, the brines were diluted by freshwater with depleted isotopic composition, which originated from the margins of Mt. Hermon in the north through the subsurface. The high-altitude source enabled the flushing and dilution of the brines, as it provided the necessary driving force to overcome the hydraulic head provided by the high density of the brines. Due to the relatively low hydraulic conductivities and limited outcrop area of the studied formations, freshwater dilution took place over geological periods and is still currently taking place.

Independent calculation of dilution factors based on salt composition and water isotopes showed higher degrees of dilution in the more permeable units (GUMF and Upper Judea Group) compared to the less permeable Taqiye Formation. This implies that brine intrusion and dilution is likely to exhibit a hysteretic behavior, where intrusion is less sensitive to hydraulic conductivities compared to subsequent flushing by freshwater (Akbarabadi and Piri 2013).

The intrusion and dilution processes were tectonically controlled. On one hand, the movement along the DSR led to the development of the subsiding basin west of the GH syncline, which accommodated the formation of the Ca-chloride brine, while on the other, the tectonic activity also led to the uplift and the exhumation of the elevated recharge areas of Mt. Hermon, which provided the necessary driving force to displace and flush the intruding brines. Flow was also assisted by the continuation of the subsiding DSR and the receding water levels of the rift lakes that enabled the gradual flushing and drainage towards the rift and the LYG.

Additionally, brine intrusion and/or subsequent dilution may have displaced or assisted in the biodegradation of the hydrocarbons that were formed during a Pliocene paleothermal event in the GH from the Mt. Scopus source rocks (Reznik and Bartov 2021). The fact that the Mt. Scopus Group is more hydrologically active than thought may provide an additional explanation to the low oil saturations found in the source rocks (Mishash and Ghareb Formation) and/or the low quality of the hydrocarbons found (mostly extremely viscous bitumen).

In summary, the unique isotopically light saline Ca-chloride water found in the DSR tectonically active basin, was deconvoluted to explain the complex mixing dynamics that took place within the hydrogeological systems of the Mt. Scopus and Judea groups in the GH: (1) subsurface intrusion of DSR brines and mixing with geochemically distinct freshwater over prolonged geological periods and (2) flushing towards the LYG natural outlets where the GH and Ajloun hydrogeological systems converge.

Appendix 1

Table 3 Locations and elevations of the studied wells, as well as the depths of the open sections sampled. The apparent hydraulic conductivity was calculated based on the bottom hole pressure readings during the drill stem tests. *X–Y* coordinates are presented in New Israel Grid units. *BGL* below ground level

Borehole	X coordinate	Y coordinate	Ground level elevation (m AMSL)	Formation	Open section depths (m BGL)	Apparent hydraulic conductivity
Ness 02	268,472	742,853	370	Ghareb-Upper Mishash boundary	997–1012	2×10^{-7}
				Ghareb	916–931	2×10^{-7}
				Taqiye	816–831	2×10^{-9}
				Lower Taqiye-Lower Mishash	850–1223	-
Ness 03	267,486	745,299	375	Ghareb	1,002–1,017	2×10^{-7}
Ness 12	275,128	763,232	635	Lower Taqiye-Lower Mishash	1,150–1,530	-
				Upper Judea Gr (Bina-Dir Hana)	1,600–1,845	-

Appendix 2

Table 4 Chemical composition and ion ratios of saline water bodies near Lake Kinneret (Kinneret brines). *X*–*Y* are New Israel Grid Coordinates

Source	Well/spring	X Coordinate	Y Coordinate	Formation	Ref	Concentration (mg/L)										Equivalent ratios		
						Na^+	K^+	Ca^{2+}	Mg^{2+}	Sr^{2+}	Cl^-	Br^-	SO_4^{2-}	HCO_3^-	TDS	Na/Cl	Mg/Ca	Ca/($HCO_3 + SO_4$)
East Kinneret brines	Bet Zayda	180,480	672,380	Quaternary fill	[a]	3,621	35.6	735	861	10.4	9,690	123	33.0	179	15,288	0.58	1.93	10.1
	1064	260,000	741,600	Quaternary fill	[a]	6,922	380	814	1,576	-	16,570	216	395	172	27,045	0.64	3.19	3.68
	1066	260,000	741,600	Quaternary fill	[a]	8,397	384	1,112	1,915	-	20,030	253	864	122	33,077	0.65	2.84	2.78
	1071	258,400	736,800	Quaternary fill	[a]	9,093	296	1,285	2,258	-	23,050	-	4.00	186	36,172	0.61	2.90	20.5
	1069	259,600	738,700	Quaternary fill	[a]	6,483	337	1,052	1,822	-	16,680	196	782	219	27,571	0.60	2.86	2.64
	1075	255,400	734,400	Quaternary fill	[a]	7,127	195	944	1,734	-	17,540	176	5.00	469	28,190	0.63	3.03	6.05
	Ha'on	258,620	736,960	Quaternary fill	[a]	4,073	178	587	896	53.4	9,883	114	244	-	16,028	0.64	2.52	5.77
West Kinneret brines	Tiberias Sp. – main	254,207	763,057	Various units	[a]	7,096	335	3,498	651	62.2	18,190	-	849	149	30,830	0.60	0.31	8.68
	Tiberias Sp. – roman	254,207	763,057	Various units	[a]	7,154	356	3,592	692	69.3	18,630	245	809	-	31,547	0.59	0.32	10.6
	Tiberias Sp. – roman	254,207	763,057	Various units	[a]	7,029	348	3,524	675	67.7	18,480	247	833	-	31,204	0.59	0.32	10.1
	Tabgha- Sartan Iver	255,756	756,105	Various units	[a]	1,420	52.3	509	144	11.9	3,075	-	260	-	5472	0.71	0.47	4.69
	Tabgha- Sartan Iver	255,756	756,105	Various units	[a]	1,293	51.0	413	134	10.9	2,765	-	233	342	5242	0.72	0.54	1.97
	Fuliya 6	248,546	748,421	Various units	[a]	7,718	305	1,912	844	-	16,260	115	2,140	224	29,518	0.73	0.73	1.98
	Fuliya new	248,550	748,420	Various units	[a]	672	22.6	228	93.0	2.90	1,323	-	172	-	2514	0.78	0.67	3.18
	Kinneret 10	249,750	745,720	Various units	[a]	8,364	293	2,081	748	38.4	17,410	126	1,940	226	31,226	0.74	0.59	2.35
	Barbutim 1020/3	249,721	745,896	Various units	[a]	1,314	55.0	523	156	-	3,070	30.0	235	341	5724	0.66	0.49	2.49
	Barbutim 48″	249,721	745,896	Various units	[b]	1,438	54.3	535	162	-	3,335	32.0	28.0	295	5879	0.66	0.50	4.92
Rosh Pina brine	Rosh Pina-1	254,207	763,057	Jurassic limestones	[a]	33,400	1160	27,000	2,920	-	105,200	1740	900	171	172,491	0.49	0.18	62.5
Seawater	MOW				[a]	10,556	380	400	1,262	13.0	18,980	65.0	2,646	140	34,442	0.86	5.20	0.35

[a]Starinsky and Katz (2014)

[b]Bergelson et al. (1999)

Table 5 Chemical composition and ion ratios of saline water bodies near the Dead Sea southern DSR brines

Source	Well/spring	Ref	Concentration (mg/L)										Equivalent ratio		
			Na^+	K^+	Ca^{2+}	Mg^{2+}	Sr^{2+}	Cl^-	Br^-	SO_4^{2-}	HCO_3^-	TDS	Na/Cl	Mg/Ca	Ca/(HCO_3+SO_4)
DSR southern lagoonary brines (northern Negev- R_o)	Boqer-1	[a]	31,080	314	15,870	1,660	427	81,060	-	1,170	-	131,581	0.59	0.17	32.5
	Kurnub-1	[a]	31,950	565	13,950	1,062	331	77,660	-	753	-	126,271	0.63	0.13	44.4
	Makhtesh Qatan-2	[a]	25,950	901	14,800	2,550	-	73,580	725	895	76	119,477	0.54	0.28	37.1
	Makhtesh Qatan-2	[a]	29,600	581	22,300	2,190	-	89,190	924	531	39	145,355	0.51	0.16	95.2
	Qeren-1	[a]	41,260	1,010	15,407	1,585	284	95,760	733	497	158	156,694	0.66	0.17	59.4
	Qeren-1	[a]	42,680	1,080	15,570	2,094	-	99,630	816	505	146	162,521	0.66	0.22	60.2
	Sherif-1	[a]	35,000	300	17,900	2,128	684	94,150	782	644	110	151,698	0.57	0.20	58.7
	Zavoa-1	[a]	36,800	408	16,500	1,960	585	92,100	730	474	14	149,571	0.62	0.20	81.5
DSR southern lagoonary brines (R_{s1})	Arava-1	[a]	50,480	1,030	50,640	12,040	1205	202,200	3,670	122	61	321,448	0.38	0.39	714
	Heimar-1	[a]	26,920	1,250	39,780	4,107	-	113,450	-	1,230	-	186,737	0.37	0.17	77.5
	Heimar-1	[a]	24,000	1,600	43,010	3,630	-	137,800	2,750	1,280	-	214,070	0.27	0.14	80.5
	Massada-1	[a]	33,800	1,000	44,340	5,034	-	144,400	2,760	352	-	231,686	0.36	0.19	302
	Massada-1	[a]	35,000	1,100	46,700	4,888	-	153,800	2,780	247	-	244,515	0.35	0.17	453
	Zuk Tamrur-3	[a]	35,570	331	20,410	5,003	937	112,200	2,610	133	-	177,194	0.49	0.40	368
DSR southern lacustrine brines (R_{s2})	Dead Sea	[a]	39,250	7,050	16,000	39,200	295	207,800	-	-	261	309,856	0.29	4.04	187
	Dead Sea	[a]	37,800	7,530	17,500	43,800	309	221,000	5,100	440	265	333,744	0.26	4.13	64.7
	Dead Sea	[a]	39,500	7,590	16,500	24,600	241	218,500	4,900	510	265	312,606	0.28	2.46	55.0
	Dead Sea	[a]	38,890	7,500	16,250	43,690	338	223,500	-	-	-	330,168	0.27	4.43	-
	Dead Sea	[a]	39,050	8,180	16,500	44,000	330	224,400	-	-	-	332,460	0.27	4.40	-
	Dead Sea	[a]	29,910	6,220	15,020	37,040	285	200,600	-	2,080	273	291,428	0.23	4.07	15.7
	Dead Sea	[a]	39,710	9,060	19,430	52,420	374	226,200	-	1,320	264	348,778	0.27	4.45	30.5
	Dead Sea	[a]	36,100	8,400	19,400	50,200	360	235,000	-	-	-	349,460	0.24	4.27	-
	Dead Sea	[a]	33,000	7,650	18,000	45,500	330	225,000	,500	2,000	-	336,980	0.23	4.17	21.6

[a]Starinsky and Katz (2014)

Appendix 3

Table 6 Isotopic composition of water bodies in the Golan Heights region

Source	Well/spring	Ref	$\delta^{18}O$ (‰ VSMOW)	$\delta^{2}H$ (‰ VSMOW)	d-excess	$^{87}Sr/^{86}Sr$
West Kinneret brines	Ein Nur	[c]	–5.70	–28.0	17.60	-
	1047	[c]	–4.50	–20.0	16.00	-
	Nur 3	[c]	–5.90	–19.0	28.20	-
	Kinneret 8	[a,c]	–2.29	–9.06	9.26	0.70772
	1020/2	[c]	–5.50	–28.0	16.00	-
	1020/3	[c]	–4.60	–27.0	9.80	-
	1020/7	[c]	–5.90	–20.0	27.20	-
	Ein Mudwara	[c]	–5.20	–22.0	19.60	-
	1051	[c]	–4.90	–25.0	14.20	-
	Kinneret 10b	[a,c]	–1.40	–2.87	8.33	0.70787
	Kinneret 5	[c]	–4.30	–9.00	25.40	-
	Kinneret 6	[c]	–1.60	–9.00	3.80	-
	Kinneret 2	[a,c]	–2.71	–14.4	7.30	0.70777
	Tiberias Roman sp.	[a,c]	–3.30	–20.0	6.40	0.70777
	CH14	[c]	–3.90	–18.0	13.20	-
East Kinneret brines	D1069	[c]	–2.30	–9.00	9.40	-
	D1071	[a,c]	–1.70	–6.00	7.60	0.70574
	Ha'on 1	[a,b]	–1.50	–8.47	3.53	0.70682
	Ha'on 2	[b]	–1.83	–10.7	3.90	-
Rosh Pina-1	Rosh Pina 3150 m	[c]	3.00	-	-	-
Lower Yarmouk Gorge- Meizar wells	Meizar 3	[d]	–6.20	–31.6	18.0	0.70767
	Meizar 3	[e]	–5.90	–33.4	13.8	0.70765
	Meizar 2	[d]	–7.16	–34.5	22.8	0.70782
	Meizar 2	[e]	–7.05	–39.0	17.3	0.70769
Lower Yarmouk Gorge- Hammat Gader thermal springs (Israel)	Ein Makla	[d]	–5.90	–28.1	19.1	0.70782
	Ein Makla	[e]	–6.22	–34.6	15.1	-
	Ein Balsam	[d]	–5.90	–30.4	16.8	0.70773
	Ein Balsam	[e]	–6.03	–29.6	18.6	-
	Ein Reach	[d]	–5.90	–30.9	16.3	0.70779
	Ein Reach	[e]	–6.06	–30.4	18.1	-
	Ein Sehina	[d]	–5.75	–23.9	22.1	-
	Ein Sehina	[d]	–5.70	–24.0	21.6	0.70775
Lower Yarmouk Gorge- Mukheiba thermal springs (Jordan)	Balsam sp.	[f]	–6.00	–29.0	19.0	-
	Maqla sp.	[f]	–6.40	–31.0	20.2	-

[a]Starinsky and Katz (2014)

[b]Bergelson et al. (1999)

[c]Gat et al. (1969)

[d]Gavrieli and Burg (2002)

[e]Israel National Water Co. (Mekorot Co.)

[f]Bajjali et al. (1997)

Appendix 4

Table 7 Chemical composition and ion ratios of water sources at the Lower Yarmouk Gorge

Source	Well/spring	Formation	Ref	Concentration (mg/L)										Equivalent ratio		
				Na^+	K^+	Ca^{2+}	Mg^{2+}	Sr^{2+}	Cl^-	Br^-	SO_4^{2-}	HCO_3^-	TDS	Na/Cl	Mg/Ca	Ca/(HCO_3 + SO_4)
Lower Yarmouk Gorge- Meizar wells	Meizar 3	Ghareb-Upper Mishash Fm	[a]	48.0	4.80	64.5	20.5	1.10	57.0	0.20	3.60	342	541	1.30	0.52	0.57
	Meizar 3	Ghareb-Upper Mishash Fm	[b]	52.0	4.20	79.0	27.0	1.08	78.0	-	20.0	352	614	1.03	0.56	0.64
	Meizar 2	Upper Judea Gr	[a]	188	21.2	169	36.8	5.00	340	4.30	305	273	1,343	0.85	0.36	0.78
	Meizar 2	Upper Judea Gr	[b]	241	25.5	175	37.4	5.20	393	5.90	315	267	1,465	0.95	0.35	0.80
Lower Yarmouk Gorge- Hammat Gader thermal springs (Israel)	Ein Makla	Various units	[a]	211	5.20	162	43.3	5.20	456	6.50	145	354	1,388	0.71	0.44	0.92
	Ein Makla	Various units	[b]	216	19.0	163	45.0	5.99	486	6.00	154	304	1,399	0.69	0.46	0.99
	Ein Balsam	Various units	[a]	134	11.5	136	36.6	3.30	282	3.40	115	349	1,070	0.73	0.44	0.84
	Ein Balsam	Various units	[b]	137	12.0	133	38.0	3.58	285	4.00	122	333	1,068	0.74	0.47	0.83
	Ein Reach	Various units	[a]	143	11.5	139	38.7	3.20	308	3.80	113	356	1,116	0.72	0.46	0.85
	Ein Reach	Various units	[b]	178	14.6	151	37.5	4.01	362	4.70	120	355	1,227	0.76	0.41	0.91
	Ein Sehina	Various units	[a]	41.0	3.20	96.5	29.6	0.50	61.5	0.30	47.6	378	658	1.03	0.51	0.67
	Ein Sehina	Various units	[a]	41.5	3.20	97.0	30.0	0.52	60.7	0.27	46.3	378	658	1.05	0.51	0.68
Lower Yarmouk Gorge- Mukheiba thermal springs (Jordan)	Balsam sp.	Various units	[c]	72.9	7.04	99.6	31.6	-	109	-	89.8	353	763	1.03	0.52	0.65
	Maqla sp.	Various units	[c]	122	12.5	118	33.4	-	198	-	158	326	968	0.95	0.47	0.68

[a]Gavrieli and Burg (2002)

[b]Israel National Water Co. (Mekorot Co.)

[c]Bajjali et al. (1997)

Appendix 5

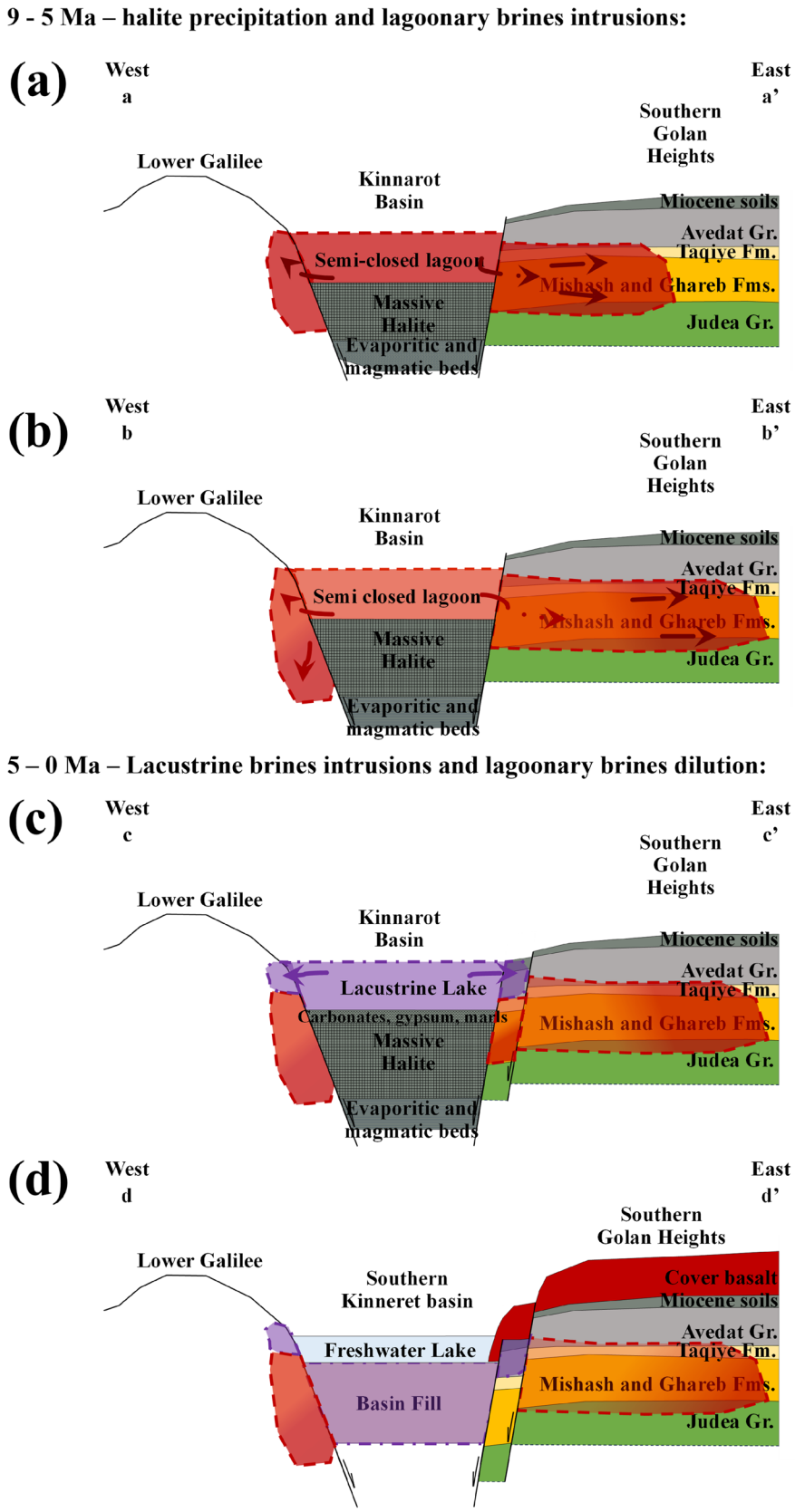

Fig. 9 Conceptual E–W cross sections demonstrating the intrusion of the DSR brines into the subsurface of GH. Based on the paleo reconstruction detailed in section 'Paleo-hydrological reconstruction'. Cross line locations are marked in Fig. 8

Acknowledgements The authors thank Genie Oil and Gas Ltd. for providing permission to use the DST data. We also thank Dr. Harold Vinegar and Dr. Scott Nguyen for fruitful discussions. Special thanks go to the Expro team and specifically to Patrick Kloth, Mathijs Hoekman, Robert Bak and Wesley Kuppen. Thank you to Lukasz Ostrowski, Annette Muffo, Edwin Koster, Aviad Levinter and Jonathan Weinberg from Baker-Hughes. We thank Iyad M. Swaed and Sabri Alian for the translation of the abstract.

Funding Open access funding provided by Geological Survey of Israel. This research was funded by the Water Authority of Israel.

Declarations

Conflicts of interest The authors declare that they have no conflict of interest in connection with the submitted material.

References

Akbarabadi M, Piri M (2013) Relative permeability hysteresis and capillary trapping characteristics of supercritical CO2/brine systems: an experimental study at reservoir conditions. Adv Water Resour 52:190–206

Al Charideh AR, Abou Zakhem B (2010) Distribution of tritium and stable isotopes in precipitation in Syria. Hydrol Sci J 55:832–843

Arad A, Bein A (1986) Saline- versus freshwater contribution to the thermal waters of the northern Jordan Rift Valley, Israel. J Hydrol 83:49–66

Aulstead KL, Spencer RJ (1985) Diagenesis of the Keg River Formation, northwestern Alberta: fluid inclusion evidence. Bull Can Pet Geol 33:167–183

Bąbel M, Schreiber BC (2014) Geochemistry of evaporites and evolution of seawater. In: Holland HD, Turekian KK (eds) Treatise on geochemistry, vol 9. Elsevier, Amsterdam, pp 483–560

Bajjali W, Clark ID, Fritz P (1997) The artesian thermal groundwaters of northern Jordan: insights into their recharge history and age. J Hydrol 192:355–382

Bergelson G, Nativ R, Bein A (1999) Salinization and dilution history of ground water discharging into the Sea of Galilee, the Dead Sea Transform, Israel. Appl Geochem 14

Bethke CM, Marshak S (1990) Brine migrations across North America: the plate tectonics of groundwater. Annu Rev Earth Planet Sci 18:287–315

Bozau E, Sattler C-D, van Berk W (2015) Hydrogeochemical classification of deep formation waters. Appl Geochem 52:23–30

Burg A, Gev I (2019) Discharge from an elevated ridge to a deep regional aquifer: a case study from Mt. Hermon, Middle East. Hydrogeol J 27(8):2803–2816

Burke WH, Denison RE, Hetherington EA, Koepnick RB, Nelson HF, Otto JB (1982) Variation of seawater$^{87}Sr/^{86}Sr$ throughout Phanerozoic time. Geology 10(10)

Carpenter AB (1978) Origin and chemical evolution of brines in sedimentary basins. SPE Annual Fall Technical Conference and Exhibition. OnePetro, Richardson, TX

Chaudhuri S, Clauer N (1993) Strontium isotopic compositions and potassium and rubidium contents of formation waters in sedimentary basins: clues to the origin of the solutes. Geochim Cosmochim Acta 57:429–437

Dafny E, Gvirtzman H, Burg A, Fleischer L (2003) The hydrogeology of the Golan basalt aquifer, Israel. Israel J Earth Sci 52:139–153

Dafny E, Burg A, Gvirtzman H (2006) Deduction of groundwater flow regime in a basaltic aquifer using geochemical and isotopic data: The Golan Heights, Israel case study. J Hydrol 330:506–524

Darrah TH, Jackson RB, Vengosh A, Warner NR, Whyte CJ, Walsh TB, Kondash AJ, Poreda RJ (2015) The evolution of Devonian hydrocarbon gases in shallow aquifers of the northern Appalachian Basin: insights from integrating noble gas and hydrocarbon geochemistry. Geochim Cosmochim Acta 170:321–355

Davisson ML, Criss RE (1996) Na-Ca-Cl relations in basinal fluids. Geochim Cosmochim Acta 60:2743–2752

Deming D, Nunn JA (1991) Numerical simulations of brine migration by topographically driven recharge. J Geophys Res: Solid Earth 96:2485–2499

Dickey PA (1969) Increasing concentration of subsurface brines with depth. Chem Geol 4:361–370

Egeberg PK, Aagaard P (1989) Origin and evolution of formation waters from oil fields on the Norwegian shelf. Appl Geochem 4:131–142

Ferguson G, McIntosh JC, Grasby SE, Hendry MJ, Jasechko S, Lindsay MB, Luijendijk E (2018) The persistence of brines in sedimentary basins. Geophys Res Lett 45:4851–4858

Fleischer L (2002) Stratigraphic table of Israel outcrops and subsurface, compilation. Plate VIII. Geological framework of the Levant. Levantine Basin and Israel 2:553–577

Flexer A, Honigstein A (1984) The Senonian succession in Israel: lithostratigraphy, biostratigraphy and sea level changes. Cretac Res 5:303–312

Freund R, Zak I, Garfunkel ZWI (1968) Age and rate of the sinistral movement along the Dead Sea Rift. Nature 220:253–255

Garfunkel Z (1981) Internal structure of the Dead Sea leaky transform (rift) in relation to plate kinematics. Tectonophysics 80:81–108

Gat JR, Mazor E, Tzur Y (1969) The stable isotope composition of mineral waters in the Jordan Rift Valley, Israel. J Hydrol 7(3):334–352

Gaupp R, Moeller P, Lüders V, di Primio R, Littke R (2008) Fluids in sedimentary basins: an overview. In: Dynamics of complex intracontinental basins: The Central European Basin System. Springer, Heidelberg, Germany, pp 345–366

Gavrieli I, Burg A (2002) Hydrological model for Golan–Ajloun Region, phase II: geochemistry of deep aquifers in the Golan Heights (in Hebrew). Rep. GSI/3/2002, Geolological Survey of Israel, Jerusalem, 23 pp

Hanor JS (1994) Origin of saline fluids in sedimentary basins. Geol Soc Lond Spec Pub 78:151–174

Hanor JS, McIntosh JC (2007) Diverse origins and timing of formation of basinal brines in the Gulf of Mexico sedimentary basin. Geofluids 7:227–237

Hardie LA (1983) Origin of CaCl2 brines by basalt-seawater interaction: insights provided by some simple mass balance calculations. Contrib Miner Petrol 82:205–213

Heimann A, Eyal M, Eyal Y (1990) The evolution of Barahta rhomb-shaped graben, Mount Hermon, Dead Sea transform. Tectonophysics 180:101–110

Heimann A, Ron H (1993) Geometric changes of plate boundaries along part of the northern Dead Sea transform: geochronologic and paleomagnetic evidence. Tectonics 12:477–491

Heimann A, Steinitz G, Mor D, Shaliv G (1996) The Cover Basalt Formation, its age and its regional and tectonic setting: implications from K-Ar and $^{40}Ar/^{39}Ar$ geochronology. Israel J Earth Sci 45:55–71

Horita J, Gat JR (1989) Deuterium in the Dead Sea: remeasurement and implications for the isotopic activity correction in brines. Geochim Cosmochim Acta 53(1):131–133

Ilani S, Rosenthal E, Kronfeld J, Flexer A (1988) Epigenetic dolomitization and iron mineralization along faults and their possible relation to the paleohydrology of southern Israel. Appl Geochem 3:487–498

Kattan Z (1997) Chemical and environmental isotope study of precipitation in Syria. J Arid Environ 35:601–615

Kattan Z (2021) Spatial mapping of atmospheric precipitation isotopes in Syria. Asian J Atmos Environ 15, Art. no. 2021009

Katz A, Starinsky A (2009) Geochemical history of the Dead Sea. Aquat Geochem 15:159–194

Kendall C, Doctor DH (2003) Stable isotope applications in hydrologic studies. Treatise Geochem 5:605

Kharaka YK, Hanor JS, Heinrich DH (2007) Deep fluids in the continents: 1. sedimentary basins. Treatise Geochem. https://doi.org/10.1016/B0-08-043751-6/05085-4

Kim JH, Ferguson G, Person M, Jiang W, Lu ZT, Ritterbusch F, Yang GM, Tyne R, Bailey L, Ballentine C (2022) Krypton-81 dating constrains timing of deep groundwater flow activation. Geophys Res Lett 49:e2021GL097618

Klein-BenDavid O, Sass E, Katz A (2004) The evolution of marine evaporitic brines in inland basins: The Jordan-Dead Sea Rift Valley. Geochim Cosmochim Acta 68:1763–1775

Kreitler CW (1989) Hydrogeology of sedimentary basins. J Hydrol 106:29–53

Land LS (1995) The role of saline formation water in crustal cycling. Aquat Geochem 1:137–145

Levitte D, Olshina A, Wachs D (1978) Geological and geophysical investigation in the Hammat Gadder Hot Springs area. Ministry of Energy and Infrastructure, Geological Survey of Israel, Jerusalem

Lowenstein TK, Hardie LA, Timofeeff MN, Demicco RV (2003) Secular variation in seawater chemistry and the origin of calcium chloride basinal brines. Geology 31:857–860

Maghrebi M, Noori R, Partani S, Araghi A, Barati R, Farnoush H, Torabi Haghighi A (2021) Iran's groundwater hydrochemistry. Earth Space Sci 8, Art. no. e2021EA001793

Marcus E, Slager J (1985) The sedimentary-magmatic sequence of the Zemah 1 well (Jordan-Dead Sea Rift, Israel) and its emplacement in time and space. Israel J Entomol 34:1–10

Margane A, Hobler M, Subah A (1999) Mapping of groundwater vulnerability and hazards to groundwater in the Irbid area, N Jordan. Zeitsch Angewand Geol 45

Margane A, Hobler M, Almomani M, Subah A (2002) Contributions to the hydrogeology of northern and central Jordan. Geologisches Jahrbuch C 68, Schweitzbart, Stuttgart, Germany

Mazor E, Mero F (1969) Geochemical tracing of mineral and fresh water sources in the Lake Tiberias Basin, Israel. J Hydrol 7(3):276–317

McArthur JM, Kennedy WJ, Chen M, Thirlwall MF, Gale AS (1994) Strontium isotope stratigraphy for Late Cretaceous time: direct numerical calibration of the Sr isotope curve based on the US Western Interior. Palaeogeogr Palaeoclimatol Palaeoecol 108(1–2):95–119

Meiler M, Reshef M, Shulman H (2011) Seismic depth-domain stratigraphic classification of the Golan Heights, central Dead Sea Fault. Tectonophysics 510:354–369

Michelson H (1979) The geology and palegeography of the Golan Heights (in Hebrew). PhD Thesis, Tel-Aviv University, Israel, 251 pp

Mimran Y, Drucman Y, Moshkovitz S, Grossowicz L, Sneh A (1985) The stratigraphy of the Mount Scopus Group in the northern Golan and its structural implications. Israel J Earth Sci 34:229–239

Mirzavand M, Ghasemieh H, Sadatinejad SJ, Bagheri R (2020) An overview on source, mechanism and investigation approaches in groundwater salinization studies. Int J Environ Sci Technol 17:2463–2476

Mor D (1993) A time-table for the levant volcanic province, according to K-Ar dating in the Golan Heights, Israel. J African Earth Sci 16(3):223–234

Neev DEKO (1967) The Dead Sea, depositional processes and environments of evaporites. Geol Survey Israel Bull 41:147

Quennell AM (1956) The structural and geomorphic evolution of the Dead Sea Rift. Q J Geol Soc 114:1–24

Raab M, Friedman GM, Spiro B, Starinsky A, Zak I (1997) The geological history of Messinian (upper Miocene) evaporites in the central Jordan Valley (Israel) and how strontium and sulfur isotopes relate to their origin. Carbonates Evaporites 12:296–324

Reznik IJ, Bartov Y (2021) Present heat flow and paleo-geothermal anomalies in the southern Golan Heights, Israel. Earth Space Sci 8(3). https://doi.org/10.1029/2020EA001299

Roded R, Shalev E, Katoshevski D (2013) Basal heat-flow and hydrothermal regime at the Golan-Ajloun hydrological basins. J Hydrol 476:200–211

Ron H, Freund R, Garfunkel Z, Nur A (1984) Block rotation by strike-slip faulting: Structural and paleomagnetic evidence. J Geophys Res: Solid Earth 89:6256–6270

Rosenberg YO, Reznik IJ (2021) Evaluating transformation of marine kerogens from Rock-Eval measurements: B. confirmation of a scaled thermal maturation path by natural samples. Organic Geochem 162:104304

Rosenberg YO, Meshoulam A, Said-Ahmad W, Shawar L, Dror G, Reznik IJ, Feinstein S, Amrani A (2017) Study of thermal maturation processes of sulfur-rich source rock using compound specific sulfur isotope analysis. Org Geochem 112:59–74

Rosenthal E, Möller P, Shentsis I, Siebert C, Magri F, Guttman J, Inbar N (2020) Natural processes determining the hydrochemistry of groundwater in the Yarmouk Basin. Environ Earth Sci 79:1–16

Rozenbaum AG, Sandler A, Stein M, Zilberman E (2019) The sedimentary and environmental history of Tortonian-Messinian lakes at the east Mediterranean margins (northern Israel). Sedimentary Geol 383(2–3):268–292

Salamon A, Hofstetter A, Garfunkel Z, Ron H (2003) Seismotectonics of the Sinai subplate: the eastern Mediterranean region. Geophys J Int 155:149–173

Satter A, Iqbal GM, Buchwalter JL (2008) Practical enhanced reservoir engineering. PennWell Corp., Tulsa, OK, pp 253–324

Shelton KL, Gregg JM, Johnson AW (2009) Replacement dolomites and ore sulfides as recorders of multiple fluids and fluid sources in the Southeast Missouri Mississippi Valley-type district: halogen-$^{87}Sr/^{86}Sr$-$\delta^{18}O$-$\delta^{34}S$ systematics in the Bonneterre Dolomite. Econ Geol 104:733–748

Shulman H, Reshef M, Ben-Avraham Z (2004) The structure of the Golan Heights and its tectonic linkage to the Dead Sea Transform and the Palmyrides folding. Israel J Earth Sci 53(3):225–237

Siebert C, Möller P, Geyer S, Kraushaar S, Dulski P, Guttman J, Subah A, Rödiger T (2014) Thermal waters in the Lower Yarmouk Gorge and their relation to surrounding aquifers. Chem Erde 74:425–441

Simon E, Shachar H, Livshitz A, Etinger H, Michelson H (1997) Development of Meizar wells field, southern Golan Heights. TAHAL, Tel Aviv, 14 pp

Sneh A (1996) The Dead Sea Rift: lateral displacement and downfaulting phases. Tectonophysics 263:277–292

Sneh A, Weinberger R (2003) Geology of the Metulla quadrangle, northern Israel: implications for the offset along the Dead Sea Rift. Israel J Earth Sci 52

Sneh A, Bartov Y, Rosensaft M, Weissbrod T (1998) Geological map of Israel, 1:200,000. GSI Rep. GSI/8/2001, Geological Survey of Israel, Jerusalem, 4 sheets

Spencer RJ (1987) Origin of CaCl brines in Devonian formations, western Canada sedimentary basin. Appl Geochem 2:373–384

Stanislavsky E, Gvirtzman H (1999) Basin-scale migration of continental-rift brines: paleohydrologic modeling of the Dead Sea basin. Geology 27:791–794

Starinsky A, Katz A (2014) The story of saline water in the Dead Sea Rift: the role of runoff and relative humidity. In: Dead Sea Transform Fault System: reviews. Springer, Heidelberg, Germany, pp 317–353

Starinsky A (1974) Relationship between Ca-chloride brines and sedimentary rocks in Israel. PhD Thesis, The Hebrew University, Jerusalem

Starinsky A, Katz A, Levitte D (1979) Temperature-composition-depth relationship in Rift Valley hot springs: Hammat Gader, northern Israel. Chem Geol 27:233–244

Stein M (2014) The evolution of Neogene-Quaternary water-bodies in the Dead Sea rift valley. In: Dead Sea transform fault system: reviews. Springer, Heidelberg, Germany, pp 279–316

Stein M (2001) The sedimentary and geochemical record of Neogene-Quaternary water bodies in the Dead Sea Basin: inferences for the regional paleoclimatic history. J Paleolimnol 26:271

Stein M, Agnon A, Katz A, Starinsky A (2002) Strontium isotopes in discordant dolomite bodies of the Judea Group, Dead Sea basin. Israel J Earth Sci 51:219–224

Stueber AM, Walter LM (1991) Origin and chemical evolution of formation waters from Silurian-Devonian strata in the Illinois basin, USA. Geochim Cosmochim Acta 55:309–325

Tahal (1989) Hydrogeological and Hydrometeorological Model of the Yarmouk Basin (in Hebrew). Rep. 01/89/62, Water Planning for Israel, Tel Aviv, 53 pp

UN (2023) United Nations geospatial map of Israel. https://www.un.org/geospatial/content/israel-2. Accessed December 2023

Walley CD (1998) Some outstanding issues in the geology of Lebanon and their importance in the tectonic evolution of the Levantine region. Tectonophysics 298:37–62

Zak I (1997) Evolution of the Dead Sea brines. Oxf Monogr Geol Geophys 36:133–144

Zak I, Bentor YK (1972) Some new data on the salt deposits of the Dead Sea area, Israel. In: Geology of saline deposits. Proc. Hannover Symp., UNESCO, Paris